HHS Public Access

Author manuscript

Cell Metab. Author manuscript; available in PMC 2024 July 11.

Published in final edited form as:

Cell Metab. 2023 July 11; 35(7): 1261–1279.e11. doi:10.1016/j.cmet.2023.04.011.

Organism-wide cell type-specific secretome mapping of exercise training in mice

Wei Wei[1,2,3,15], **Nicholas M. Riley**[3,4,5,15], **Xuchao Lyu**[1,3,14,15], **Xiaotao Shen**[6], **Jing Guo**[7], **Steffen H. Raun**[8], **Meng Zhao**[1,9,10], **Maria Dolores Moya-Garzon**[1,3], **Himanish Basu**[11], **Alan Sheng-Hwa Tung**[1,3], **Veronica L. Li**[1,3,4], **Wentao Huang**[12,13], **Amanda L. Wiggenhorn**[1,3,4], **Katrin J. Svensson**[1,9,10], **Michael P. Snyder**[6,9,10], **Carolyn R. Bertozzi**[3,4,5], **Jonathan Z. Long**[1,3,9,10,14,*,#]

[1]Department of Pathology, Stanford University School of Medicine, Stanford, CA 94305 USA

[2]Department of Biology, Stanford University, Stanford, CA 94305 USA

[3]Sarafan ChEM-H, Stanford University, Stanford, CA 94305 USA

[4]Department of Chemistry, Stanford University, Stanford, CA 94305 USA

[5]Howard Hughes Medical Institute, Stanford University, Stanford, CA 94305 USA

[6]Department of Genetics, Stanford University School of Medicine, Stanford, CA, 94035 USA

[7]Department of Microbiology and Immunology, Stanford University School of Medicine, Stanford, CA 94305 USA

[8]Department of Biomedical Sciences, University of Copenhagen, Denmark

[9]Stanford Diabetes Research Center, Stanford University School of Medicine, Stanford, CA 94305 USA

[10]Cardiovascular Institute, Stanford University School of Medicine, Stanford, CA 94305 USA.

[11]Department of Immunology, Harvard Medical School, Boston, MA 02115 USA

[12]Whitehead Institute for Biomedical Research, Cambridge, MA, 02142 USA

[13]Department of Biology, Massachusetts Institute of Technology, Cambridge, MA, 02142 USA

[14]Wu Tsai Human Performance Alliance, Stanford University, Stanford, CA 94305 USA

[15]These authors contributed equally

[*]To whom correspondence should be addressed. jzlong@stanford.edu.

[#]Lead contact

Author Contributions

Conceptualization, W.W., N.M.R., and J.Z.L.; methodology, W.W., N.M.R., and X.L.; investigation, W.W., N.M.R., X.L., X.S., S.H.R., J.G., M.Z., M.D.M.G., H.B., A.T., V.L.L., W.H., and A.L.W.; writing – original draft, W.W., N.M.R., and J.Z.L.; writing – review & editing, W.W., N.M.R., X.L., and J.Z.L.; resources, J.Z.L., C.R.B., K.J.Z., and M.P.S.; supervision and funding acquisition, J.Z.L. and C.R.B.

Declaration of Interests

Stanford University has filed a provisional patent on extracellular CES2 proteins and methods of use.

Summary

There is great interest to identify blood-borne factors that mediate tissue crosstalk and function as molecular effectors of physical activity. Although past studies have focused on an individual molecule or cell type, the organism-wide secretome response to physical activity has not been evaluated. Here, we use a cell type-specific proteomic approach to generate a 21-cell type, 10-tissue map of exercise training-regulated secretomes in mice. Our dataset identifies >200 exercise training-regulated cell type-secreted protein pairs, the majority of which have not been previously reported. *Pdgfra*-cre-labeled secretomes were the most responsive to exercise training. Lastly, we show anti-obesity, anti-diabetic, and running performance-enhancing activities for proteoforms of intracellular carboxylesterases whose secretion from the liver is induced by exercise training.

eTOC blurb:

• Wei *et al.* use proteomics to identify cellular secretomes changes in response to exercise training at organism-wide scale. Using this dataset, Wei *et al.* identified an exercise-inducible secreted protein from the liver that enhances exercise performance and improves metabolic health.

Graphical Abstract

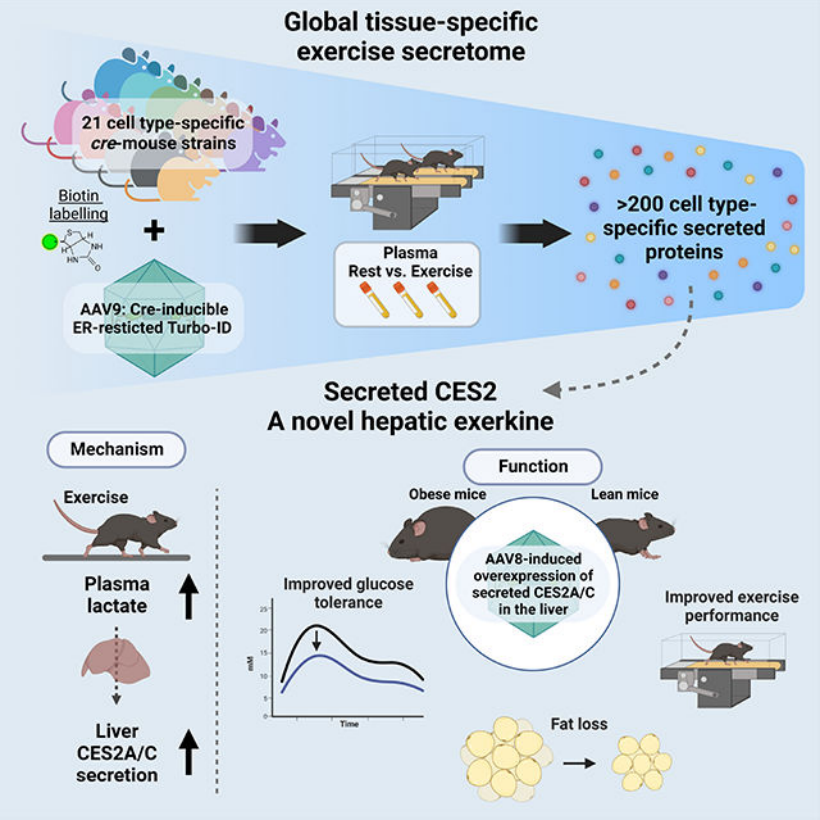

Keywords

Exercise; secretome; tissue crosstalk; hepatokine; cell type; energy metabolism

Introduction

Physical activity is a powerful physiologic stimulus that provides benefits to many organ systems and confers protection against disease[1,2]. Conversely, physical inactivity is a major contributor to cardiovascular morbidity and mortality[3,4]. The magnitude of the benefits of physical activity is comparable, and in some cases even greater, than currently available first-line pharmacological treatments[5–7]. The mechanisms responsible for the benefits of exercise are incompletely understood, but likely extend beyond activity-associated increases in energy expenditure alone[8,9].

In recent years, there has been tremendous interest in the identification and characterization of exercise-inducible, soluble (e.g., secreted) blood-borne molecules. These circulating molecules, which have been called “exerkines” or “exercise factors,” are secreted signaling molecules that function as molecular effectors of physical activity[10,11]. Over 50 years ago, Goldstein[12] demonstrated that contracting muscle from dogs produced a humoral factor that stimulated glucose uptake when transferred to non-exercised muscle preparations. More recently, experiments involving re-infusion of exercise-conditioned plasma in mice have also provided additional evidence for bioactive molecules present in the circulation following exercise[13,14].

At a molecular level, many individual candidate metabolites, lipids, polypeptides and proteins have been proposed to function as exerkines[15–24]. However, these previous efforts have typically focused on a single factor (e.g., IL-6) and/or a single cell type/tissue of origin (e.g., muscle). Few studies have systematically mapped exercise-inducible secreted molecules across an entire organism. A major challenge, especially for secreted polypeptides and proteins, has been the low depth of plasma proteome coverage by classical shotgun proteomics techniques[25]. Aptamer- and antibody-based approaches provide higher sensitivity, but are not comprehensive for the plasma proteome and cannot be used to detect the array of potentially new proteoforms or cleavage fragments that might be produced following physical activity[17,26]. Finally, many secreted proteins are expressed by multiple cell types, and single snapshot detection of these molecules in the circulation would not be expected to enable detection of cell type-specific, and potentially bidirectional regulation of exercise-inducible changes across distinct cell types.

We[27,28] and others[29–31] have recently described a biochemical secretome profiling methodology that enables direct labeling, enrichment, and identification of secreted proteins in mice at a cell type-specific resolution. Key to this methodology is the delivery of an engineered biotinylation enzyme TurboID[32] into the secretory pathway of cells via adeno-associated virus (AAV) transduction. Cell type-specific labeling is achieved genetically because the expression of the TurboID is restricted to those cells expressing cre recombinase. Biotinylated and secreted plasma proteins can then be purified directly from blood plasma using streptavidin beads and analyzed by LC-MS/MS. Our initial secretome studies with the proximity biotinylation approach previously established that cell type-specific secretome changes could be profiled directly in an intact animal[28]. Here, we have extended this secretome profiling to organism-wide scale and examined the cell type-specific secretome response to exercise training. Our organism-wide 21-cell type, 10-

tissue secretome map of physical activity provides fundamental insights into the molecular identity and cellular origin of exercise training-regulated circulating factors and illuminates the dynamic regulation of intercellular and inter-organ crosstalk by physical activity.

Results

Study design and proteomic map of exercise training-regulated secretomes

The experimental design for organism-wide, cell type-specific secretome profiling in response to exercise training is shown schematically in Fig. 1A. First, we generated adeno-associated adenovirus serotype 9 (AAV9) expressing a cre-inducible, endoplasmic reticulum-restricted TurboID (AAV9-FLEx-ER-TurboID, 3*10e11 GC/mouse, intravenously) (Fig. 1A and see **Methods**). In cells expressing cre recombinase, inversion of the FLEx cassette results in robust expression of the ER-TurboID construct. AAV9 was chosen since this serotype exhibits broad tissue distribution and transduction[33]. Next, we assembled 21 manually-curated hemizygous cre mouse driver lines from the Jackson Laboratories (N = 6/genotype, Fig. 1A, see **Methods**). Included amongst the set of cre driver lines were those that target specific organs previously shown to participate in response to exercise training (e.g., *MCK*-cre targeting muscle, *Adiponectin*-cre targeting fat, and *Albumin*-cre targeting liver). Other cre drivers exhibited well-validated expression patterns (e.g., *Lysm*-cre for macrophages), even though those cell types had not been previously implicated in the response to physical activity. In the cases where tamoxifen-inducible cre driver lines were used, tamoxifen (2 mg/mouse, intraperitoneally) was administered two weeks after viral transduction. As expected, robust *TurboID* mRNA expression was detected in tissues from all transduced mice compared to virally-transduced, wild-type control mice (Fig. S1A and see **Methods**). Furthermore, we harvested a collection of tissues from a subset of cre driver mice in which TurboID expression was predicted to occur in an organ-restricted manner (*Albumin*-cre for liver, *Ucp1*-cre for brown fat, *Adiponectin*-cre for all adipose, *MCK*-cre for muscle, *Myh6*-cre for heart, *Pdx1*-cre for pancreas, and *Syn1*-cre for brain). V5-tagged TurboID protein, as measured by Western blot using an anti-V5 epitope tag antibody, was robustly detected with the expected organ-restricted pattern (Fig. S1B).

Given the expansive scope of our initial proteomic survey, we reasoned that performing our initial proteomic studies in a single sex would be most reasonable approach and most useful for downstream data analysis. Male mice were virally transduced for 3-weeks to allow for robust TurboID expression across cell types. Then mice were separated into treadmill running or sedentary groups (N = 3 per group per genotype, Fig. 1A). Our one-week treadmill running protocol, adapted from Wu et al.,[34], consisted of running for 60 min/day at a speed of 20 m/min. To control for potential perturbations of circadian rhythms, control sedentary mice were also transferred to the same room as the exercise training animals (see **Methods**). After the one-week treadmill training protocol, mRNA levels of *Pgc1a* and *Nr4a1* in quadriceps muscle were consistently induced by on average 1.6-fold and 1.3-fold respectively across all animals (Fig. S1C, D)[35–37]. Total inguinal white adipose tissue mass was reduced by 30% in the exercise group (sedentary: 333 ± 11 mg; exercise: 237 ± 11 mg, mean ± SEM, $P < 0.001$) (Fig. S1E). Histological analysis of the inguinal adipose tissue also showed reduced adipocyte size (Fig. S1F). Additionally, exercised animals of all genotypes

exhibited −0.68 ± 0.02 g (mean ± SEM, N = 66) weight change during the 1-week treadmill running whereas the sedentary controls (N = 66) gained +0.50 ± 0.02 g (mean ± SEM, N = 66, Fig. S1G). This body weight difference was in part due to slightly reduced food intake (Fig. S1H). Taken together, these molecular and physiologic data validate both the secretome labeling mouse lines as well as the one-week exercise training protocol.

To determine the identity of exercise training-regulated secreted proteins and their cell types of origin, we supplemented biotin to mice for the final three days of the exercise training protocol to biotinylate in vivo secretomes (Fig. 1A, right, and S1I, see **Methods**). Two hours after the final bout of running, blood plasma was collected from each mouse and biotinylated secreted proteins were purified using streptavidin beads, digested following an S-trap protocol, and analyzed by LC-MS/MS in data-independent acquisition (DIA) mode (see **Methods**). We chose to use a previously described spectrum library-free DIA approach that relies on gas-phase fractionation (GPF)-DIA data from a pooled sample to generate DIA-only chromatogram libraries[38,39]. This allowed us to search all data against experiment-specific chromatogram libraries using the freely available EncyclopeDIA platform[38], followed by further processing in the Skyline and Perseus data analysis environments[40,41]. Because our dataset provides information about both secreted proteins and cell types, we define a “cell type-protein pair” as a set [protein, cell type] which indicates the detection of that secreted protein in the indicated cell type secretome. To filter for bona fide cell type-protein pairs enriched by streptavidin, we also applied a 1.5-fold enrichment filter for each cell type-protein pair versus non-transduced, wild-type controls (see **Methods**). In total across all samples (N = 3 mice/condition × 2 conditions × 21 genotypes), we detectd 1,272 unique cell type-protein pairs with >= 2 peptides detected in all 3 replicates of both conditions (Table S1).

Exercise training-regulated cell type-protein pairs were identified by comparison of differential secreted proteins from the same cell type in sedentary versus exercised mice. This comparison also provides a natural control for differing levels of proximity labeling enzyme expression and/or varying levels of secretome biotinylation between distinct cell types. Exercise training significantly altered 256 cell type-protein pairs consisting of 181 unique proteins changed across 21 cell types (20.1% of the entire dataset, adjusted P-value < 0.05 and exercise fold change > 1.5, Fig. 1B and Table S1), many of which have not been previously described. Fewer unique proteins (N = 181) than all exercise training-regulated cell type-protein pairs (N = 256) were observed because the same protein can be secreted by more than one cell type. We identified several example candidates of exercise training-regulated secreted proteins selectively altered in one cell type (Fig. 1C–F). For instance, two carboxylesterases, CES2A and CES2C, were increased by 3-fold exclusively in secretomes from *Albumin*-cre mice following treadmill running (Fig. 1C, D). CES2 enzymes are classically annotated as intracellular, liver-enriched endoplasmic reticulum resident proteins. Nevertheless, our data suggest that CES2 enzymes can also be released from the liver in an exercise training-dependent manner. Other well established secreted protein-cell type pairs, such as the hormone adiponectin from fat cells (ADIPOQ in *Adipoq*-cre transduced secretomes)[42], was robustly detected in our dataset but not regulated by physical activity (Fig. 1E). Finally, one of the most exercise training-inducible cell type-protein pairs in

the dataset was TIMP3 from *Pdgfra*-cre labeled secretomes (Fig. 1F). While TIMP3 had previously been implicated in diverse physiologic roles including in myogenesis[43], thermogenesis and metabolism[44], vascular remodeling[45], and atherogenesis[46], its exercise training-inducible secretion from *Pdgfra*-cre labeled cells has not been previously identified. We conclude that one week of treadmill running in mice results in specific modulation of a subset of secreted proteins-cell type pairs across our entire secretome dataset.

Systematic analysis of exercise training-regulated cell type-secreted protein pairs

The distribution of these exercise training-regulated cell type-protein pairs across the 21 cell types is shown in Fig. 2A. We observed an average and median of 12 and 10, respectively, proteins changed per cell type secretome in response to exercise training, with a range across all cell types of 1 to 44. The number of proteins changed in each cell type secretome by exercise training was not simply correlated to secretome size since the two cell types with the largest number of unique proteins identified in their secretomes (*Albumin*-cre, with 142 proteins, and *MCK*-cre, with 132 proteins) exhibited near the median number of exercise training-regulated secreted protein changes (Fig. 2A). All cell types exhibited some secretome changes following exercise training, demonstrating that all cell types exhibit exercise training responsiveness to some degree as measured by changes to their production of soluble factors. Approximately half of the exercise training-regulated secretome changes (50%, 129 out of 256) were observed in only one cell type (Fig. 2B). In addition, the frequency of either exercise training up- or down-regulated proteins was equivalent (66 proteins increased and 63 proteins decreased, Fig. 2B), suggesting that exercise training regulation of soluble factors does not only involve production of new secreted molecules, but also suppression and other regulation of active protein secretion. The other half of the exercise training-regulated secretome changes (50%, 127 out of 256) were proteins expressed in multiple cell types that exhibited cell type-specific regulation following exercise training. In this latter group, bidirectional change, defined as up-regulation in one cell type and down-regulation in a different cell type, was commonly observed (40%). These data further underscore the increased resolution afforded by cell type-specific secretome profiling, as well as the need to use global approaches for evaluating exercise training-induced changes, which are complex, bidirectional, and cell type-specific.

For proteins that were secreted by more than one cell type, we also observed interesting patterns of cell type-specific responses to exercise training (Fig. 2C–F). For instance, LOXL1, a secreted enzyme involved in extracellular protein lysine oxidation, was selectively downregulated following exercise training in secretomes from *Pdgfra*-, *Nr5a1*-, and *Lysm*-cre transduced mice (Fig. 2C). Conversely, the extracellular matrix protein EMIL1 was upregulated following exercise training selectively in *Col1a1*, *Lysm* and *Nr5a1*-cre secretomes (Fig. 2D). We also identified several examples of proteins expressed in multiple cell types and bidirectionally regulated by exercise training. These include SOD3 (upregulated in *MCK*-cre and *Pdgfra*-cre, and downregulated in *Pdx1*-cre secretomes) (Fig. 2E) and HSP7C (upregulated in *Vil1*-cre and *Lck*-cre, and downregulated in *Pdgfra*-cre and *UCP1*-cre secretomes) (Fig. 2F). A bubble plot visualizing all such examples of exercise training-regulated secreted proteins with regulation in >= 2 secretomes is shown in Fig. 2G. While several of these proteins have been identified as exercise training-regulated proteins

in the literature, our dataset further contextualizes and refines their interpretations at a cell type level. For instance, total plasma SOD3 was previously reported to be induced by acute treadmill running in humans as well as voluntary wheel running and treadmill exercise training in mice[47–50]. However, only one of these previous studies suggested that muscle is a cellular origin for exercise training-inducible SOD3[48]. Our dataset not only confirms upregulation of SOD3 secretion from muscle following exercise training, but also identifies *Pdgfra* and *Pdx1* as additional cell types that express SOD3 and contribute to the exercise training-inducible regulation of this protein (Fig. 2E). Similarly, PEDF is a neurotrophic growth factor widely expressed across multiple cell types. In humans, circulating PEDF is reduced after a single bout of cycling[51] as well as after 12-month moderate-intensity aerobic exercise training[52]. PEDF was downregulated in our dataset in both *Nr5a1*-cre and *Pdgfra*-cre secretomes (Fig. 2G), suggesting that these two cell types contribute to the downregulation of plasma PEDF after exercise training. Finally, we manually queried each of the proteins changed at least in one cell type in our study (in total 181 proteins) for any prior knowledge of exercise training regulation. Only ~24% of these factors were known to be regulated by exercise training, and 6 of such proteins had clear cell type/tissue of origin (Table S2). Collectively, our dataset provided more than 200 previously unknown cell type-secreted protein pairs that are under exercise training regulation.

Secretomes from *Pdgfra*-cre labeled cells are highly responsive to exercise training

While metabolic cell types (muscle, liver, and fat) have typically been examined in the context of exercise training, our dataset indicated that *Pdgfra*-cre labeled secretomes were amongst the most exercise training-responsive, as measured by the number of exercise training-regulated proteins (Fig. 2A). As an alternative method for determining magnitude of the exercise training response, we also developed a direct “exercise training-responsiveness” metric for each cell type secretome in our dataset (see **Methods**). This metric takes into account magnitude and statistical significance of the exercise training-regulated changes, as well as the secretome size of that cell type. *Pdgfra*-cre labeled secretomes once again emerged as the most responsive cell type (exercise training-responsiveness score = 115.4 and Fig. 3A).

Pdgfra-cre labeled cells are a population of anatomically-distributed cells that have been described in the literature as fibroblasts, mesenchymal stem cells, or progenitor/precursor cells[53–55]. They have diverse roles in tissue remodeling, fibrosis and cell proliferation depending on the resident tissue and physiological context[53,54]. To understand the organ localization of the *Pdgfra*-cre labeled cells labeled in our secretome labeling experiments, we measured *TurboID* mRNA across multiple tissues from *Pdgfra*-cre transduced mice (Fig. S2A). Robust *TurboID* mRNA enrichment was detected across many tissues examined, including lung, adipose tissues (inguinal and brown), muscle, gut, kidney, and brain (Fig. S2A). This distribution is similar to the reported expression of *Pdgfra* mRNA across tissues and suggest that *Pdgfra* localized to multiple organs are participating in the exercise training-regulated secretome response detected in our dataset (Fig. S2B).

The entire secretome of *Pdgfra*-cre labeled cells is shown in Fig. 3B. A diverse array of secreted proteins with pleiotropic physiologic functions were found to be regulated

by exercise training. Some of the most upregulated molecules included the previously mentioned TIMP3 (17-fold) and SOD3 (5-fold), as well as the S100 family member S10AB (5-fold), the HDL-binding protein VIGLN (4-fold), and the vitamin B12 transport protein TCO2 (3-fold). Conversely, downregulated secreted proteins in the *Pdgfra*-cre secretome included ER-resident proteins such as the protein disulfide isomerase PDIA4 (87% suppression) and ER calcium ATPase AT2A3 (88% suppression), the growth factor PEDF (81% suppression), and the lipid metabolizing enzyme PAFA (69% down). Gene ontology analysis revealed enrichment of several biological pathways in the exercise training-regulated *Pdgfra*-cre secretome, of which the highest scoring by gene ratio was "response to stimulus" (P = 4.96E-07, gene ratio = 0.77, Fig. 3C). Additional biological processes identified from the *Pdgfra*-cre secretome included "response to stress" (P = 2.00E-06, gene ratio = 0.45), and "response to organic substance" (P = 1.03E-04, gene ratio = 0.34) (Fig. 3C). These observations suggest that *Pdgfra*-cre labeled cells respond to exercise training by sensing exercise training-regulated environmental cues, such as metabolites, cytokines, or other signaling molecules, that in turn drive bidirectional changes in the *Pdgfra*-cre labeled secretome.

We next sought to validate some of the *Pdgfra*-cre secretome responses using an orthogonal method, as well as to determine whether the secretome changes of *Pdgfra*-labeled cells are dependent on the duration of training. Towards this end, we used Western blotting with commercially available antibodies to determine the levels of three exercise-regulated secreted proteins (F13A, C4BPA and ITIH2) from the *Pdgfra*-cre secretome in a new cohort of virus-transduced, *Pdgfra*-cre mice. In our original proteomic dataset, F13A, C4BPA, and ITIH2 were found to be 4-, 2-, and 4-fold upregulated in *Pdgfra*-cre secretomes after 1 week treadmill running. In this time course experiment, transduced animals (N = 3/group) were separated into four groups: sedentary, acute exercise (single treadmill bout, 20 m/min for 60min), 3-day or 7-day exercise training (daily treadmill running, 20 m/min for 60 min) (Fig. 3D). As shown in Fig. 3E and S2C, Western blotting revealed that all three proteins were robustly elevated from 7-day treadmill running cohorts. Interestingly, while ITIH2 exhibited a similar magnitude upregulation after 1-day, 3-day and 7-day running, the upregulation of F13A was specific to 7-day running. On the other hand, C4BPA was down-regulated at both 1-day and 3-day treadmill running, and upregulated in the 7-day group, indicating this protein is suppressed after acute exercise but increased after chronic training (Fig. 3E and S2C). These data demonstrate that the exercise training-regulated proteins in the *Pdgfra*-cre secretome are robust across multiple cohorts and are dependent on the frequency of exercise training.

Finally, we sought to determine potential sex-dependent responses in the *Pdgfra*-cre labeled secretome. A new cohort of female *Pdgfra*-cre mice was transduced with TurboID virus (AAV9-FLEx-ER-TurboID, 3*10e11 GC/mouse, intravenously) and secretomes were profiled by shotgun proteomics as described above. Interestingly, *Pdgfra*-cre male and female secretomes exhibited both overlapping and distinct exercise training responses (Fig. S2D and E, and Table S3). For instance, the sex-independent exercise training-responsive proteins once again included the dramatic elevations in both TIMP3 and F13A (13- and 5-fold increase, respectively) and strong suppression of PEDF, CLUS and LOXL1 (83%, 73% and 34% reduction, respectively). Sex-dependent *Pdgfra*-cre secretome changes included

induction of VWF only in females (20-fold) and induction of ITIH2 only in males (4-fold). We conclude that sex influences the *Pdgfra-cre* labeled secretome response to exercise training.

In vitro studies of lactate-stimulated protein secretion

Two of the most robust exercise training-inducible molecules from the *Albumin*-cre labeled secretome belonged to the same family of carboxylesterase enzymes (CES2A and CES2C, Fig. 4A). Because hepatocytes can be easily cultured and manipulated in vitro, we used the *Albumin*-cre/CES2 cell type-protein pair as a representative molecular handle to investigate the molecular drivers of this process in vitro.

To first validate the exercise training-inducible secretion of CES2 proteins from the liver, we used a commercially available pan anti-CES2 antibody to probe streptavidin-purified blood plasma from a separate cohort of TurboID-transduced and exercise trained *Albumin*-cre mice. This commercially available anti-CES2 antibody exhibited the expected immunoreactivity to purified, recombinantly produced CES2A and CES2C proteins (Fig. S3A). As expected, extracellular CES2 levels from streptavidin-purified *Albumin*-cre secretomes were increased after exercise training. (Fig. 4B). The total hepatocyte secretome biotinylation signal remained unchanged (Fig. S3B), establishing equivalent secretome protein loading. We therefore conclude that CES2 secretion from the liver is a robust molecular event in response to one week of treadmill running.

We sought to test the hypothesis that lactate might serve as an exercise training-inducible extracellular signal that stimulates CES2 secretion from hepatocytes. This hypothesis was based on the well-established increase in lactate flux through the liver via the Cori cycle, as well as our previous experiments showing that other metabolic fuels (e.g., fatty acids) can stimulate protein secretion from the liver[28]. We also confirmed that circulating lactate level was increased 3-fold in mice subjected to our 1-week treadmill running protocol compared to sedentary controls (N = 5/condition) (Fig. S3C). To test this lactate regulator hypothesis, primary hepatocytes were treated with lactate (2 mM, 4 h) and extracellular CES2 proteins were measured by Western blotting in both cell lysates and conditioned medium. As additional controls, we tested a variety of other exercise training-regulated organic acids, including pyruvate, acetate, malate, fumarate, beta-hydroxybutyrate, kynurenate, and pantothenate[20–22,56,57]. As shown in Fig. 4C, lactate treatment robustly increased the levels of extracellular CES2. Pyruvate, a structurally similar metabolite, also increased CES2 secretion, though with a slightly lower magnitude than that of lactate. By contrast, none of the other metabolites tested increased extracellular CES2 levels (Fig. 4C and Fig. S3D), establishing that only extracellular lactate, and to a lesser extent pyruvate, exhibit CES2 secretion stimulatory activity.

A dose response of lactate revealed increased CES2 secretion at >1 mM lactate levels (Fig. 4D), whereas intracellular CES2 levels were unchanged at all concentrations of lactate tested. In addition, the effect of lactate to induce secretion of CES2 was specific since extracellular albumin levels were unchanged with lactate treatment (Fig. S3E). This lactate-induced CES2 secretion is cell type-specific since exogenous expression of CES2A in HEK293T cells resulted in complete retention of this protein intracellularly and treatment of

lactate (1–50 mM, 4 h) concentration did not induce the release of CES2A into conditioned medium (Fig. S3F). Reduced CES2 secretion was observed when hepatocytes were concurrently treated with lactate (2 mM, 4 h) and an inhibitor of vesicle transport, brefeldin A (BFA 5 μg/ml, 4 h), establishing that these CES2 proteins are released extracellularly via the classical secretory pathway (Fig. 4E, and Fig. S3G). Lastly, because lactate import into hepatocytes is critical for this metabolite to function as a substrate in the Cori cycle, we next tested whether lactate import via the monocarboxylate transporters (MCTs) was required for induction of CES2 protein secretion. Treatment of primary hepatocytes with AR-C155858, a nanomolar dual MCT1/2 inhibitor[58,59], dose-dependently inhibited the lactate-induced secretion of CES2 (Fig. 4F). Once again, the inhibitory effect of AR-C155858 was selective for CES2, since no changes were observed in extracellular albumin under these conditions (Fig. S3H). These data demonstrate that extracellular lactate is sufficient to drive secretion of CES2 proteins via classical pathway from hepatocytes in vitro in a manner that requires import of lactate into hepatocytes (Fig. 4G).

Secreted CES2 proteins exhibit anti-obesity, anti-diabetic, and endurance-enhancing effects in mice

We sought to determine whether release of extracellular CES2 from the liver following exercise was simply a response to exercise training, or whether soluble CES2 proteins might function as circulating molecular effectors of physical activity. Supporting a potential functional role for extracellular CES2, three prior studies showed that liver-specific overexpression of either human or mouse CES2 lowered body weight, reduced hepatic steatosis, and improved glucose homeostasis[60–62]. An intestine-specific transgenic CES2C mouse model also exhibited a similarly improved metabolic phenotype[63]. However, these prior studies did not consider the possibility that extracellular CES2, which is likely also increased in addition to elevation of intracellular CES2 in these transgenic models, might in part mediate the anti-obesity, anti-steatosis, and anti-diabetic phenotypes observed. In addition, whether CES2 proteins might improve exercise endurance or performance had not been previously evaluated.

To directly test the functional role extracellular CES2 in energy metabolism and glucose homeostasis without a confounding contribution from intracellular CES2, we set out to generate an engineered version of CES2 that would be exclusively localized extracellularly (Fig. 5A). Analysis of the primary amino acid sequences for both murine CES2A and CES2C proteins revealed an N-terminal signal peptide, a central alpha/beta hydrolase superfamily domain with the catalytic active site GXSXG motif, and a C-terminal HXEL motif (X=A for CES2A, and R for CES2C). Previous studies showed that the C-terminal HXEL motif is indispensable for the ER lumen localization and C-terminal deleted version of CES2 can be readily detectable in the conditioned medium of cancer cells[64–66]. We therefore generated CES2A/C constructs in which the HXEL amino acids were removed from the C-terminus (CES2-ΔC) (Fig. 5A). An additional N-terminal Flag epitope tag was included after the signal peptide to aid downstream detection. Both wild-type CES2 and CES2-ΔC constructs were transfected into HEK293T cells and the CES2 protein localization was determined by Western blotting of cell lysates and conditioned media. As expected, full-

length CES2A/C were enriched intracellularly, whereas both CES2A-ΔC and CES2C-ΔC proteins were exclusively found extracellularly (Fig. S4A).

To deliver the engineered soluble CES2 proteins to mice, we generated adeno-associated virus (serotype 8) expressing each of our two engineered CES2A-ΔC and CES2C-ΔC constructs. CES2-ΔC was driven under the control of the hepatocyte-specific thyroxine binding protein (*Tbg*) promoter to achieve liver-specific expression (Fig. 5B). Notably, we[67] and others[68,69] have previously shown that the pattern of expression under the *Tbg* promoter is largely overlapping to that of the *Albumin*-cre. Next, mice were transduced with AAV-*Tbg*-CES2A-ΔC or AAV-*Tbg*-CES2C-ΔC (N = 10/group, 10e11 GC/mouse, intravenously). Control mice were transduced with an equal titer of AAV-*Tbg*-GFP. As expected, Western blotting of blood plasma using an anti-Flag antibody revealed elevation of circulating CES2A-ΔC and CES2C-ΔC (Fig. 5C), which was further validated by measuring plasma ester hydrolysis activity using a previously reported synthetic substrate of carboxylesterases (Fig. S4B). In contrast to blood plasma, we did not observe significant changes in total liver CES2 protein level as shown by the anti-Flag and anti-CES2 antibody staining (Fig. S4C and D) nor an increase in liver ester hydrolysis activity (Fig. S4E). These data confirm that our viral constructs increase only extracellular CES2A and CES2C levels without affecting the intracellular levels of CES2.

One week after viral transduction, mice were placed on high-fat diet (HFD, 60% kcal from fat). Over the subsequent 7 weeks, both CES2A-ΔC and CES2C-ΔC groups of mice exhibited reduced body weight compared to mice transduced with AAV-*Tbg*-GFP (GFP: 45.4 ± 0.8 g versus CES2A-ΔC 41.5 ± 0.9 g and CES2C-ΔC 41.8 ± 0.8 g, mean ± SEM) (Fig. 5D). Food intake over this time period was unaltered, suggesting that the lower body weights are not simply due to reduced caloric intake (Fig. 5E). In the 7th week, glucose and insulin tolerance tests revealed improved glucose clearance and insulin sensitivity in both CES2A-ΔC and CES2C-ΔC groups (Fig. 5F and G). Dissection of tissues at the end of the experiment revealed significant reductions of inguinal white adipose tissue (iWAT) (23% and 38% reduction for CES2A-ΔC and CES2C-ΔC, respectively, vs GFP) and epididymal adipose tissue (eWAT) mass (18% and 29% reduction for CES2A-ΔC and CES2C-ΔC, respectively, vs GFP) (Fig. 5H and I). The lean mass of all three groups remained unchanged (Fig. 5H), establishing the effects on body weight are due to reduced adiposity and not any changes in lean mass. Taken together, we conclude that extracellular CES2 proteins have functions in energy balance and glucose homeostasis that are independent of their intracellular roles in triglyceride hydrolysis.

Next, we sought to understand the energy balance pathways driving the anti-obesity effects of mice overexpressing CES2A-ΔC and CES2C-ΔC. We therefore used metabolic chambers to measure parameters of whole-body energy intake and expenditure in a new cohort of virus-transduced mice. Importantly, the metabolic chamber measurements were performed at a time point prior to the divergence in body weights (3 weeks for CES2C-ΔC and 5 weeks for CES2A-ΔC) (Fig. S4F and G). Both CES2A-ΔC and CES2C-ΔC overexpressing mice exhibited significantly augmented VO_2 (Fig. S4H and I) without any effects on food intake and respiratory exchange ratio (Fig. S4J–M). Interestingly, increased movement was observed in mice overexpressing CES2A-ΔC, but not CES2C-ΔC (Fig. S4N and O). We

conclude that the anti-obesity effect of CES2A-ΔC and CES2C-ΔC are in part due to increased whole-body energy expenditure, but via distinct physiologic mechanisms.

Quantitative mRNA analysis of limb muscles revealed broad changes in mRNA expression of genes related to cellular metabolism, fiber type and ER Ca^{2+}-handling (Fig. S4P–R). Metabolic genes such as *Pgc1a*, *PDHa1*, *Tfam* and *HKII* were also robustly induced in tibialis anterior muscles of CES2A-ΔC mice (Fig. S4P). We therefore next measured running speed and running endurance in CES2A-ΔC and CES2C-ΔC overexpressing animals. We transduced a new cohort of mice with AAV-*Tbg*-CES2A-ΔC, AAV-*Tbg*-CES2C-ΔC or AAV-*Tbg*-GFP (N = 8–10/group, 10e11 GC/mouse, intravenously). Over a 7-week period in which mice were fed with chow instead of high fat diet, body weights and food intake were unchanged by (Fig. S5A and B). Glucose and insulin tolerance tests at this time point also showed no significant differences between three groups of mice on chow diet (Fig. S5C and D). At 8 weeks, we conducted maximal running speed tests using previously established protocols[70,71] (see **Methods**). Mice overexpressing CES2A-ΔC, but not CES2C-ΔC, exhibited a robust 15% increase in maximal running speed, 25% increase in running time, and consequently a 34% increase in total running distance compared to GFP-transduced control mice ($P < 0.001$, Fig 5J–L). Dissection of tissues at the end revealed consistent reductions of iWAT mass (19% and 12% reduction for CES2A-ΔC and CES2C-ΔC, respectively, vs GFP) and eWAT mass (26% and 29% reduction for CES2A-ΔC and CES2C-ΔC, respectively, vs GFP). The lean mass of all three groups remained unchanged (Fig. S5E). Taken together, we conclude that overexpression of CES2A-ΔC, but not CES2A-ΔC also mimics the trained phenotype and improves running speed and endurance.

Lastly, to explore if the metabolic improvements from elevated soluble CES2 can be additive to exercise training's effects, we prepared a new cohort of virally-transduced mice and started chronic exercise training 5 weeks on these mice 4-weeks after HFD feeding (N = 5–6/group, AAV-*Tbg*-GFP sedentary, AAV-*Tbg*-GFP exercise, AAV-*Tbg*-CES2A-ΔC sedentary, AAV-*Tbg*-CES2A-ΔC exercise, AAV-*Tbg*-CES2C-ΔC sedentary, AAV-*Tbg*-CES2C-ΔC exercise) (see **Methods**). 1-month chronic exercise training alone induced a very strong anti-obesity effect in all three groups of mice (sedentary versus exercise: GFP 42.9 ± 0.9 g vs 35.8 ± 0.3 g, CES2A-ΔC 37.3 ± 0.8 g vs 33.7 ± 1.1 g, CES2C-ΔC 37.5 ± 0.6 g vs 32.1 ± 1.5 g) (Fig. S5F–J). We further observed a statistically significant, additive effect of further suppression of obesity with CES2C-ΔC, but not CES2A-ΔC overexpression (Fig. S5F). Similarly, in a glucose tolerance test, exercise training in combination with CES2C-ΔC was additive, whereas exercise training in combination with CES2A-ΔC was not (Fig. S5H). However, this additivity for exercise CES2C-ΔC and was not observed in the insulin tolerance test (Fig. S5I). We conclude that certain metabolic benefits associated with overexpression of CES2C-ΔC, but not CES2A-ΔC, are additive with exercise training.

The anti-obesity effects of soluble CES2 proteins requires enzyme activity

Are the enzymatic activities required for the any of the physiologic functions of soluble CES2 proteins? To answer this question, we generated enzymatically dead versions of wildtype CES2-ΔC (CES2A-ΔC-S227A and CES2C-ΔC-S230A respectively). We validated complete loss of enzymatic activities of these mutant proteins using activity assays

measuring hydrolysis of the prototypical artificial substrate 4-nitrophenyl acetate (Fig. S6A). Next, we cloned these two genes into AAV-*Tbg* vectors and transduced a new cohort of mice (N=10/group, AAV-*Tbg*-CES2A-ΔC, AAV-*Tbg*-CES2A-ΔC-S227A, AAV-*Tbg*-CES2C-ΔC, AAV-*Tbg*-CES2C-ΔC-S230A or AAV-*Tbg*-GFP, 10e11 GC/mouse, intravenously). Western blotting of blood plasma using an anti-Flag antibody revealed similar expression level between wildtype and mutant CES2A-ΔC and CES2C-ΔC respectively (Fig. S6B), demonstrating unchanged protein secretion and stability of wild-type and mutant proteins in blood plasma. One week after viral transduction, mice were placed on high-fat diet (HFD, 60% kcal from fat). Over the subsequent 9 weeks, as expected both CES2A-ΔC and CES2C-ΔC groups of mice exhibited reduced body weight compared to mice transduced with AAV-*Tbg*-GFP (GFP: 50.5 ± 1.0 g versus CES2A-ΔC 44.8 ± 1.1 g and CES2C-ΔC 45.0 ± 0.7 g, mean ± SEM). The catalytic activity of the soluble CES2 proteins was required for this effect since both mutant groups exhibited identical body weight to control high fat diet-fed mice (CES2A-ΔC-S227A 49.5 ± 0.7 g and CES2C-ΔC-S230A 49.0 ± 1.0 g, mean ± SEM) (Fig. 6A). Food intake was not changed amongst all groups of mice (Fig. S6C).

To understand potential substrates of soluble CES2 proteins that might be downstream effectors of their anti-obesity effects, we performed untargeted metabolomics on plasma from CES2A-ΔC, CES2C-ΔC, or GFP-transduced mice (see **Methods**). Differential peaks were identified by XCMS, and lipid structural assignments were made using the METLIN database[72]. A total of 462 metabolite features were changed by elevated soluble CES2C (43.6% of total detected features, adjusted P-value < 0.05, FC >1.5, versus GFP) whereas soluble CES2A exhibited modest effects on 15 features (1.6% of total detected features, adjusted P-value < 0.05, FC >1.5, versus GFP) (Fig. 6B and Table S4). Interestingly, ~30% of changed metabolite features were annotated as lipids, such as phosphatidylserine (PS), phosphatidylethanolamine (PE), phosphoinositide (PI), phosphatidylcholine (PC), ceramide and acylglycerol (Fig. 6B). These data suggest that soluble CES2C-ΔC induces profound alterations in the circulating lipid species that correlate with its anti-obesity effects, whereas the anti-obesity effects of CES2A-ΔC are not correlated with as widespread dysregulation of plasma lipid species. These data further provide evidence that CES2A-ΔC and CES2C-ΔC exert their anti-obesity effects via distinct mechanistically pathways.

Discussion

Here we have generated an organism-wide proteomic dataset of the cell type-specific secretome responses to one week of treadmill running. In contrast to previous efforts that have focused on individual secreted factors or individual cell types, our current dataset provides several insights of potential importance to our understanding of cell and tissue crosstalk during physical activity, including 1) the demonstration that ~20% of cell type-protein pairs exhibit complex, bidirectional, and cell type-specific regulation following exercise training; 2) the identification of *Pdgfra* cells as a highly responsive cell type to exercise training; 3) evidence that the production of non-canonical secreted proteoforms contributes to exercise training-regulated tissue crosstalk; and 4) discovery of secreted CES2 as extracellular enzymes with anti-obesity, anti-diabetic, and endurance-enhancing functions.

Classically, muscle has been studied as a principal source of activity-inducible “myokines” that mediate tissue crosstalk in exercise training. More recent evidence has expanded this model to include exercise training-inducible hepatokines from the liver[73] and adipokines from the fat[23]. In general, many of these past studies have focused on individual cell types. Our studies suggest that many more cell types respond to exercise training than previously recognized, including *Pdgfra*+ cells distributed to multiple organ systems. Recent reports using single cell RNA-sequencing showed that exercise training regulation in adipose was most strongly pronounced in adipose stem cells[74], which are defined by the expression of *Pdgfra*+[75]. These adipose-resident fibroblasts may indeed correspond to a subset of the *Pdgfra*+ cells identified in our secretome profling dataset. In the future, it will be important to specifically determine which exercise training-regulated cell types and in which organs beyond adipose are defined by *Pdgfra*+ expression.

40% of multi-origin secreted proteins detected in our study exhibit bidirectional change after exercise training, meaning that their secretion is up-regulated in certain cell types following exercise training and downregulated in others. The cell type-specific nature of this regulation underscores the importance of cell type-specific resolution for the analysis of complex perturbations, rather than bulk measurements from total plasma. Currently, why the same protein can have different directionality after exercise training in different cell types remains unknown. We speculate that one possibility is due to cell type-specific differences in the response to exercise training-regulated hormones, which may functionally result in different intracellular regulation of the secretory pathway in a cell type-dependent manner. Mechanistic dissection of these differences could provide important clues to the cell type-specific responses of exercise training.

Several lines of evidence suggest that the cell type-specific changes found in our dataset indeed reflect bulk changes to circulating protein levels. For instance, we can find specific examples of exercise training-inducible proteins that have been reported in the literature by bulk plasma measurements, and which are also changed in our dataset (e.g., TIMP3[76], SOD3[47–50]). Nevertheless, future studies to understand the correlation of biotinylated protein levels with total plasma protein levels at a global scale will only be enabled by higher sensitivity, targeted shotgun proteomics or aptamer-based arrays that can be used for mouse plasma proteins.

Using cell culture systems, we also provide evidence that the exercise training-inducible secretion of CES2 from the liver can be recapitulated by addition of extracellular lactate to primary hepatocytes in vitro. While the precise downstream mechanism linking lactate import to protein secretion from hepatocytes remains unknown, we suspect one likely possibility includes lactate-inducible proteolytic cleavage of the CES2 C-terminus. This C-terminus contains the ER retention signal required for intracellular localization of CES2. In addition, RHBDL4 has been proposed as a hydrolase that liberates an array of ER-resident proteins into the extracellular space[77]. Consistent with this idea, we were unable to detect peptides corresponding to C-terminus of either CES2A or CES2C (Fig. S6D). Such an ER-retention signal cleavage mechanism may also explain the secretion of several other ER-resident proteins in our dataset, such as H6PD (in *Adiponectin*-cre secretomes), CALX (in *Albumin*-cre and *Lysm*-cre secretomes) and AT2A1 (in *MCK*-cre secretomes). The

possibility that lactate itself constitutes a more general mechanism linking physical activity to secreted protein-mediated tissue crosstalk remains an open question for future work.

We also provide evidence that exercise training-inducible secretion of CES2 proteins is not simply a molecular response to exercise training. Instead, using engineered versions of CES2 that are localized exclusively extracellularly, we show that soluble CES2 proteins exhibit anti-obesity, anti-diabetic, and performance-enhancing actions in mice. The anti-obesity and anti-diabetic observations here further refine the interpretation of previous CES2 transgenic models: whereas those previous mouse models likely induced both intracellular and extracellular CES2 proteins, our exclusively extracellular CES2A-ΔC and CES2C-ΔC constructs demonstrate that circulating CES2 proteins are sufficient to reproduce at least some of the metabolically beneficial phenotypes. In addition, the ability for CES2A-ΔC, but not CES2C-ΔC to enhance running speed and endurance was a novel finding. Lastly, the *CES2* locus has been linked to multiple cardiometabolic parameters in the UK Biobank, including HDL cholesterol (P = 5.14e-311, beta = +0.0625), blood pressure (P = 1.64e-17, beta = +0.0317), and BMI-adjusted waist-hip ratio (P = 4.61e-15, beta = −0.0297), suggesting that exercise training-regulated soluble CES2 proteins might also impact cardiometabolic health in humans.

The variation of detectable *TurboID* mRNA across different tissues suggest varying secretome labeling efficiencies amongst cell types. Several reasons likely contribute to this variation, including differential AAV transduction efficiency between cell types, as well as the isolation of total organ mRNA when potentially only a small number of particular target cell types are transduced. Notably, we are only comparing the effect of exercise training within the same Cre transduced line (e.g., each Cre serves as its own control) and therefore avoid the confounding factor of varying TurboID expression. Transgenic TurboID mice will be a valuable resource in future works to standardize and increase labeling efficiency, especially in non-transducible cell types.

Projecting forward, an important extension of this work will be to understand the effects of different exercise training regimes and training time on the cellular secretomes in vivo. Which of the secretome responses observed here are specific to the training protocol used in this study, and which might be general responses to multiple types of exercise training? Our time course of *Pdgfra*-cre secretomes in response to exercise training already provides evidence that the secretome responses can be complex and time-dependent. Indeed, a single bout versus multiple bouts of either aerobic or resistance training produces distinct phenotypic responses that correlate with activation of overlapping yet distinct molecular pathways[81,82]. On the other hand, our identification of a functional coupling between lactate and CES2 secretion from the liver suggests that soluble CES2 may be a molecular effector more generally associated with multiple and distinct modalities of physical activity. In addition, these murine datasets will need to be compared with studies of exercise plasma in large and deeply phenotyped human cohorts[83,84] to determine which molecular changes might be conserved or species-specific. Ultimately, we anticipate that these and other organism-wide datasets will provide a systematic foundation for probing the role of secreted proteins as mediators of tissue crosstalk in exercise training and as molecular effectors of physical activity across the diverse cell and organs systems across the body.

Limitations of the study

We acknowledge several limitations of this study. Firstly, there may be other mechanisms regulating a secreted protein's circulating levels beyond secretion alone, including proteolytic degradation and/or other clearance mechanisms. Consequently, our dataset may also contain "false-negatives" (e.g., bona fide exercise training-inducible proteins) because of these additional regulatory mechanisms for circulating proteins. Secondly, our secretome dataset does not distinguish between which molecular changes are acute versus adaptive. Thirdly, the use of a 1-week treadmill running perturbation in this study leads to the activation of exercise training markers in the skeletal muscle, as well as a slight reduction in body weight, fat mass, and food intake in mice. Although these phenotypes are commonly associated with exercise training, it is not possible to determine the individual contribution of each factor to the changes detected in the secretome. Fourthly, our studies have not performed any loss-of-function studies that selectively ablate extracellular, but not intracellular CES2 functions. The discovery and development of neutralizing CES2 antibodies would enable these important studies. Fifthly, there remains possibility for sex-specific secretome effects in cell types beyond *Pdgfra*+ cells, which would be an area of potentially interesting future study. Finally, our treadmill running was performed in the morning, corresponding to the early rest phase in mice. Although this experimental condition may potentially activate a circadian rhythm-dependent secretome response, the detected changes in the secretome are likely attributable to the exercise training itself, as both the sedentary control and exercise training animals were similarly perturbed. Additionally, no changes in individual proteins derived from hepatocytes, such as CES2, were observed due to the disruption of circadian rhythm (data not shown). On the other hand, growing evidence suggests interplay and crosstalk between exercise training and circadian rhythms[22,78–80]. Our secretome profiling approach may be useful for providing high resolution profiling in future studies that seek to dissect the relationship between exercise and circadian rhythms.

STAR Methods

Resource availability

Lead contact.—Further information and requests for reagents may be directed to and will be fulfilled by the lead contact Dr. Jonathan Z. Long (jzlong@stanford.edu).

Materials availability.—Further information and requests for reagents will be fulfilled by Dr. Jonathan Z. Long (jzlong@stanford.edu). A list of critical reagents (key resources) is included in the key resources table. Material that can be shared will be released via a Material Transfer Agreement.

Data and code availability.

- The mass spectrometry proteomics data have been deposited to the ProteomeXchange Consortium via the PRIDE partner repository with the dataset identifier PXD034535[86]. Processed data from these outputs are available as Supplemental Data files. Uncropped blots and values of graphs are included in the zip file, Data S1.

- This paper does not report original code.
- Any additional information required to reanalyze the data reported in this paper is available from the lead contact upon request.

Experimental models and subject details

Mouse models.—Animal experiments were performed according to procedures approved by the Stanford University IACUC. Mice were maintained in 12 h light-dark cycles at 22 °C and ~50% relative humidity and fed a standard irradiated rodent chow diet. Where indicated, high fat diet (Research Diets, D12492) was used. C57BL/6J male and female mice (stock no. 000664), homozygous *Alb*-cre male mice (stock no. 003574), hemizygous *Cdh16*-cre male mice (stock no. 012237), homozygous *Gcg*-icre mice male mice (stock no. 030663), hemizygous *Pdx1*-cre male mice (stock no. 014647), homozygous *Myh6*-creER male mice (stock no. 005657), hemizygous *MCK*-cre male mice (stock no. 006475), hemizygous *Myh11*-icreER male mice (stock no. 019079), homozygous *Cdh5*-cre male mice (stock no. 006137), heterozygous *Pdgfra*-creER male and female mice (stock no. 032770), homozygous *Pdgfrb*-creER male mice (stock no. 030201), hemizygous *Vil1*-cre male mice (stock no. 021504), homozygous *Sftpc*-creER male mice (stock no. 028054), hemizygous *Col1a1*-creER male mice (stock no. 016241), hemizygous *CD2*-cre male mice (stock no. 008520), hemizygous *Lck*-cre male mice (stock no. 003802), hemizygous *Nr5a1*-creER male mice (stock no. 033687), hemizygous *Nes*-creER male mice (stock no. 016261), hemizygous *Syn1*-cre male mice (stock no. 003966), hemizygous *Adipoq*-cre male mice (stock no. 028020), hemizygous *Ucp1*-cre male mice (stock no. 024670), and hemizygous *LysM*-cre male mice (stock no. 031674) were purchased from Jackson Laboratory. All the cre driver male mice were crossed with female C57BL/6J mice to generate hemizygous/heterozygous mice. Genotypes were verified following genotyping protocols and using the primers listed on the Jackson Laboratory website. The reported Cre tissue expression pattern from Jackson Laboratory and detected tissue expression was shown in Table S5.

Methods details

Cell line cultures.—HEK293T cells were obtained from ATCC (CRL-3216) and cultured in complete medium (Dulbecco's Modified Eagle's Medium, Corning, 10013CV; 10% FBS, Corning, 35010CV; 1:1,000 penicillin–streptomycin, Gibco, 15140–122). Cells were grown at 37 °C with 5% CO_2. For transient transfection, cells were transfected in 10 cm^2 at ~60% confluency using PolyFect (Qiagen, 301107) and washed with complete medium 6 h later.

Western blotting.—For analyzing samples using Western blot, proteins were separated on NuPAGE 4–12% Bis-Tris gels and transferred to nitrocellulose membranes. Equal loading was ensured by staining blots with Ponceau S solution. Blots were then incubated with Odyssey blocking buffer for 30 min at room temperature and incubated with primary antibodies (1:1000 dilution mouse anti-V5 antibody (Invitrogen, R960–25), 1:1000 dilution mouse anti-FLAG antibody (Sigma, F1804), 1:5000 dilution rabbit anti-β-tubulin antibody (Abcam, ab6046), 1:1000 dilution rabbit anti-CES2 antibody (Novus Biologicals, NBP1–91620), 1:500 rabbit anti-TIMP3 antibody (Thermo Fisher, 710404), 1:500 rabbit anti-F13A antibody (MyBioSource, MBS2026456), 1:500 rabbit anti-ITIH2 (MyBioSource,

MBS9612213), 1:500 dilution rabbit anti-C4BPA (Abnova, H00000722-D01P), 1:5000 dilution goat anti-albumin antibody (Novus biological, NB600–41532), 1:1000 dilution rabbit anti-H6PD antibody (Abcam, ab170895), 1:1000 dilution rabbit anti-BHMT (Abcam, ab96415), 1:1000 dilution streptavidin Alexa Fluor 680 (Thermo Fisher, S32358)) in blocking buffer overnight at 4 °C. Blots were washed three times with PBST (0.05% Tween-20 in PBS) and stained with species-matched secondary antibodies (1:10000 dilution goat anti-mouse IRDye 680RD (LI-COR, 925–68070), 1:10000 dilution goat anti-rabbit IRDye 800RD (LI-COR, 925–68070), 1:10000 dilution donkey anti-goat IRDye 800CW (LI-COR, 925–32214)) at room temperature for 1 h. Blots were further washed three times with PBST and imaged with the Odyssey CLx Imaging System. Secondary antibodies were not required for imaging blots incubated with streptavidin Alexa Fluor 680 primary antibody.

AAV production.—pAAV-FLEx-ER-TurboID (Addgene, 160857), pAAV-*Tbg*-CES2A-ΔC, pAAV-*Tbg*-CES2C-ΔC, pAAV-*Tbg*-CES2A-ΔC-S227A and pAAV-*Tbg*-CES2C-ΔC-S230A plasmids were amplified, extracted using an endotoxin-free Qiagen Maxiprep kit (Qiagen, 12362) and sequence verified. AAV9-FLEx-ER-TurboID (60221S), AAV8-*Tbg*-CES2A-ΔC (63849S), AAV8-*Tbg*-CES2C-ΔC (63850S), AAV8-*Tbg*-CES2A-ΔC-S227A (V7929S) and AAV8-*Tbg*-CES2C-ΔC-S230A (V7928S) viruses were made with Penn Vector Core.

Viral transduction.—For transduction of brain-specific cre driver lines (*Syn1*-cre and *Nes*-creER mice), injection was carried out as previously reported[87]. Briefly, postnatal day 1 pups were anesthetized on ice for 30–60 s. The temporal vein was identified under a dissection microscope and injected with 10e11 genome copies (GC) of AAV9-FLEx-ER-TurboID virus per mouse diluted in a total volume of 30 μl saline (containing 0.3 μl 0.4% Trypan blue solution) with a 31G syringe (BD, 328290). Injected pups were then recovered in hands for 30 s and returned to home cages. For *Syn1*-cre mice, 8 to 9 weeks after injection, 1-week treadmill running was performed as described below on male mice with the correct genotype. For *Nes*-creER mice, 5 to 6 weeks after injection. Tamoxifen (Sigma, T5648–1G) was prepared as a 20 mg/ml solution in corn oil and administered daily for 5 d (100 μl per day, intraperitoneally) to induce recombination. 3 weeks after the final tamoxifen injection, 1-week treadmill running was performed on male mice with the correct genotype. For transduction of cre/icre driver mice (except *Syn1*-cre mice), 6-week-old male hemizygous mice were injected via tail vein with a 29G syringe (Thermo Fisher, 14-841-32) at a dose of 3*10e11 GC per mouse diluted in saline in a total volume of 100 μl per mouse. Three weeks after transduction with the AAV9-FLEx-ER-TurboID virus, 1-week treadmill running was performed. For transduction of creER/icreER mice (except Nes-creER mice), AAV9-FLEx-ER-TurboID virus was injected via tail vein into 6-week-old hemizygous/heterozygous male mice at a dose of 3*10e11 GC per mouse. After a 2-week transduction period, tamoxifen (Sigma, T5648–1G) was prepared as a 20 mg/ml solution in corn oil and administered daily for 5 d (100 μl per day, intraperitoneally) to induce recombination. After the final tamoxifen injection, mice were housed in their home cages for 3 additional weeks before performing 1-week treadmill running. For transduction of C57BL/6J mice, AAV8-*Tbg*-CES2A-ΔC/CES2C-ΔC/GFP viruses were injected via tail vein

into 8 to 10-week-old male mice at a dose of 10e11 GC per mouse. One week after viral transduction, mice were fed with HFD (60% fat, Research Diets, D12492). Body weights and food intake were measured every week. After 6 weeks of HFD feeding, glucose tolerance and insulin tolerance tests were performed. At the end of 7 weeks of HFD feeding, tissues and blood were collected for further analysis.

Mouse exercise and secretome labeling protocols.—A 6-lane animal treadmill (Columbus Instruments, 1055-SRM-D65) was used for mouse running. Prior to treadmill running, the bodyweight of individual mice was measured with a tabletop scale. Mice were then acclimated to the treadmill for 5 minutes before running at a speed of 5 m/min for 5 min. Then the speed was increased to 20 m/min and kept constant for 60 min. A serological pipette was used to manually stir the mice to avoid excessive electrical shock during the whole running period. After exercise, mice were returned to home cages. The sedentary control animals were kept in their home cages but removed from the original racks and put next to the treadmill. These mice were constantly disturbed by the noises from the running animals and treadmill. Running was performed for 7 consecutive days in the morning (between 9–12 am). On the fourth day of one-week treadmill running, biotin water (0.5 mg/ml) was supplemented to initiate labeling and kept accessible to mice until the end of the experiment. On the next day, an additional dose of biotin was administered by injection (24 mg/ml, intraperitoneally, in a solution of 18:1:1 saline:Kolliphor EL:DMSO, final volume of 200 μl per mouse per day) 1 h prior to the running for 3 consecutive days. Sedentary animals received biotin delivery the same as exercise animals.

Quantitative PCR.—We collected the following tissues from the indicated genotypes: liver from *Alb*-cre mice, heart from *Myh6*-creER and *Myh11*-icreER mice, brain from *Syn1*-cre and *Nes*-creER mice, iWAT from *Adipoq*-cre mice, BAT from *Ucp1*-cre mice, lung from *Sftpc*-creER, *Pdgfra*-creER, *Pdgfrb*-creER and *Cdh5*-cre mice, quadricep muscle from *MCK*-cre mice, intestines from *Vil1*-cre mice, pancreas from *Gcg*-icre and *Pdx1*-cre mice, kidney from *Cdh16*-cre mice, adrenal gland from *Nr5a1*-cre mice, hind limb with muscles removed from *Col1a1*-creER mice. For *Lck*-cre and *CD2*-icre mice, splenocytes were collected by passing the spleen through a cell strainer (Corning, 352350) and resuspended in 2% BSA solution. Splenocytes were stained with FITC anti-mouse TCRβ (BioLegend, 109206), Percp/Cy5.5 anti-mouse CD19 (BioLegend, 152406) and LIVE/DEAD Aqua (Invitrogen, L34957). αβT cells from *Lck*-cre mice were gated on Aqua-CD19−TCRβ+, isolated with FACS, and spun down at 300 g for 5 min at 4 °C for downstream analysis. For *CD2*-icre mice, αβT cells were gated on Aqua-CD19−TCRβ+ and B cells were gated on Aqua-CD19+TCRβ−. Both αβT cells and B cells were sorted with FACS, mixed, and spun down at 300 g for 5 min at 4 °C for downstream analysis. For *Lysm*-creER mice, a new cohort of 6 to 8-week old mice (N = 3) was transduced with AAV9-FLEx-ER-TurboID virus and was injected with tamoxifen to induce cre recombination the same as described before. 3 weeks after the final tamoxifen injection, 1 ml 3% (w/v) thioglycolate solution (Thermo Fisher, B11716) was intraperitoneally injected. 5 days later, 10 ml ice-cold DPBS (Thermo Fisher, 14190144) was intraperitoneally injected to isolate the accumulated macrophages in the peritoneal cavity. Cells were spun down at 400 g for 10 min at 4 °C for downstream analysis. Isolated cells or 30–50 mg of frozen tissues were added to bulk tubes (Thermo

Fisher,15340162) containing metal beads and 1 ml TRIzol Reagent (Invitrogen, 15596026). Tissues were then homogenized using a Benchmark BeadBlaster Homogenizer at 4 °C. The mixture was spun down at 13,000 rpm for 10 min at 4 °C to pellet the insoluble materials. RNA was extracted using a RNeasy Mini Kit (Qiagen, 74106) and reverse-transcribed using a High-Capacity cDNA Reverse Transcription Kit (Thermo Fisher, 4368813). Quantitative PCR was performed using Ssoadvance Universal SYBR Green mix (Biorad, 1725272) with a CFX Opus Real-Time PCR instrument. All values were normalized by the ΔΔCt method to *Rps18*. Primer sequences used are described in Key resources table.

Plasma and tissue sample preparation from mice.—2 h after the final bout of running (time point is 4 h after the biotin intraperitoneal injection and is the same for both sedentary and exercise animals), blood was collected via submandibular bleeding using a 21G needle (BD, 305129) into lithium heparin tubes (BD, 365985) and immediately spun down at 5,000 rpm for 5 min at 4 °C to retrieve the plasma fractions. All tissues were dissected, weighed on a scale, collected into Eppendorf tubes, and immediately frozen on dry ice and stored at −80 °C. Adipose tissues were collected into 4% paraformaldehyde for histology analysis. For western blot analysis, tissues were mixed with 0.5 ml of cold RIPA buffer and homogenized using a Benchmark BeadBlaster Homogenizer at 4 °C. The mixture was spun down at 13,000 rpm for 10 min at 4 °C to pellet the insoluble materials. The supernatant was quantified using a tabletop Nanodrop One and analyzed by western blot. To remove remaining biotin from blood plasma, 200 µl plasma from a single mouse was added with 15 ml PBS and subsequently concentrated 30-fold using 3 kDa filter tubes (Millipore, UFC900324) by spinning down at 4,000 rpm for 1 h. The flowthrough was discarded, and the dilution and centrifugation steps were repeated until a final solution of 500 µl was retrieved at a 9000-fold final dilution. To enrich biotinylated plasma proteins, 200 µl Dynabeads MyOne Streptavidin T1 magnetic beads (Thermo Fisher, 65602) were washed twice with 1ml washing buffer (50 mM Tris-HCl, 150 mM NaCl, 0.1% SDS, 0.5% sodium deoxycholate, 1% NP-40, 1 mM EDTA, 1× HALT protease inhibitor, 5 mM trolox, 10 mM sodium azide and 10 mM sodium ascorbate) and resuspended in 100 µl washing buffer. The beads were then added to the 500 µl biotin-free plasma solution and incubated at 4 °C overnight with rotation. The beads were subsequently washed twice with 1 ml washing buffer, once with 1 ml 1 M KCl solution, once with 1 ml 0.1 M Na_2CO_3 solution, once with 1 ml 2 M urea in 10 mM Tris-HCl (pH 8.0), and twice with 1 ml washing buffer. Eppendorf tubes containing beads were vortexed for 3s between each step to ensure thorough washing. Finally, biotinylated proteins were eluted by boiling at 95 °C for 10 min in 60 µl of 2× sample buffer supplemented with 20 mM DTT and 2 mM biotin. Successful enrichment of biotinylated plasma proteins was validated by running the elution sample on NuPAGE 4–12% Bis-Tris gels followed by silver staining (Thermo Fisher, LC6070) according to the instructions from the manufacturer's protocol.

Proteomic sample processing.—After cooling down to room temperature for 3 min, boiled streptavidin-purified plasma samples (60 µl) were digested using a Mini S-Trap protocol provided by the manufacturer (Protifi, C02-micro-80). As previously described[27], cysteine residues were first alkylated by incubating in 30 mM iodoacetamide (Sigma, A3221) in the dark at room temperature for 30 min. Samples were then acidified with

phosphoric acid at a final concentration of 1.2%. 420 µl bind/wash buffer (100 mM tetraethylammonium bromide (TEAB) in 90% methanol) was added to each sample. 150 µl samples were loaded onto micro S-trap columns and spun down at 4000 g for 20 s. The flow-through was discarded, and the centrifugation step was repeated until all the solution passed through the column. Following four washes with 150ul bind/wash buffer, 1 µg trypsin (Promega, V5113) was added to the S-trap and incubated at 47 °C for 90 min. After trypsinization, peptides were washed once with 50 mM TEAB (40 µl), once 0.2% formic acid (40 µl), once with a mixture of 50% acetonitrile and 0.2% formic acid (40 µl) and once of 0.2% formic acid in water (40 µl) by spinning down at 1,000g for 60 s. Eluted fraction from each wash was combined, lyophilized, resuspended in 0.2% formic acid, normalized to concentration using a Nanodrop Spectrophotomerter (Thermo Fisher, absorbance at 205 nm), and analyzed by LC-MS/MS. One microliter of each sample was taken and combined into a pooled sampled that was used to make the chromatogram library.

Proteomics data acquisition.—Proteomics data were acquired using a spectrum-library free DIA approach that relies on gas-phase fractionation (GPF) to generate DIA-only chromatogram libraries[38,39]. Peptides were separated over a 25 cm Aurora Series Gen2 reverse-phase LC column (75 µm inner diameter packed with 1.6 µm FSC C18 particles, Ion Opticks). The mobile phases (A: water with 0.2% formic acid and B: acetonitrile with 0.2% formic acid) were driven and controlled by a Dionex Ultimate 3000 RPLC nano system (Thermo Fisher). An integrated loading pump was used to load peptides onto a trap column (Acclaim PepMap 100 C18, 5 um particles, 20 mm length, Thermo Fisher) at 5 µl/minute, which was put in line with the analytical column 5.5 minutes into the gradient. The gradient was held at 0% B for the first 6 minutes of the analysis, followed by an increase from 0% to 5% B from 6 to 6.5 minutes, and increase from 5 to 22% B from 6.5 to 66.5 minutes, an increase from 22% to 90% from 66.5 to 71 minutes, isocratic flow at 90% B from 71 to 75 minutes, and re-equilibration at 0% B for 15 minutes for a total analysis time of 90 minutes per acquisition. Eluted peptides were analyzed on an Orbitrap Fusion Tribrid MS system (Thermo Fisher). Precursors were ionized was ionized with a spray voltage held at +2.2 kV relative to ground, the RF lens was set to 60%, and the inlet capillary temperature was held at 275 °C.

Six chromatogram library files were collected through six repeated injections of the pooled sample only. Here, the instrument was configured to acquire 4 m/z precursor isolation window DIA spectra using a staggered isolation window pattern[88] from narrow mass ranges using window placements optimized by Skyline. DIA MS/MS spectra were acquired with an AGC target of 400,000 charges, a maximum injection time of 54 ms, beam-type collisional dissociation (i.e., HCD) with a normalized collision energy of 33, and a resolution of 30,000 at 200 m/z using the Orbitrap as a mass analyzer. The six gas-phase fractionation chromatogram libraries were collected with nominal mass ranges of 400–500 m/z, 500–600 m/z, 600–700 m/z, 700–800 m/z, 800–900 m/z, and 900–1000 m/z. The exact windowing scheme was downloaded from https://bitbucket.org/searleb/encyclopedia/wiki/Home [39] and is available in Supplementary Information here. Precursor MS1 spectra were interspersed every 25 scans with an AGC target of 400,000 charges, a maximum injection time of 55 ms, a resolution of 60,000 at 200 m/z using the Orbitrap as a mass analyzer, and a scan range of

either 395–505 m/z, 495–605 m/z, 595–705 m/z, 695–805 m/z, 795–905 m/z, or 895–1005 m/z.

For quantitative samples (i.e., the non-pooled samples) the instrument was configured to acquire 25 × 16 m/z precursor isolation window DIA spectra covering 385–1015 m/z using a staggered isolation window pattern with window placements optimized by Skyline (windowing scheme downloaded from the same link as above and available as Supplementary Information here). DIA spectra were acquired with the same MS/MS settings described above. Precursor MS1 spectra were interspersed every 38 scans with a scan range of 385–1015 m/z, an AGC target of 400,000 charges, a maximum injection time of 55 ms, and a resolution of 60,000 at 200 m/z using the Orbitrap as a mass analyzer. The detailed parameters were recorded in Table S6. The mass spectrometry proteomics data have been deposited to the ProteomeXchange Consortium via the PRIDE partner repository with the dataset identifier PXD034535.

Proteomics data analysis to generate cell type-protein pairs.—Staggered DIA spectra were demultiplexed from raw data into mzML files with 10 ppm accuracy using MSConvert[89] with settings described in Pino et al[39]. Encyclopedia (version 1.12.31)[38] was used to search demultiplexed mzML files using an internal PECAN fasta search engine called Walnut[90] and a reviewed-plus-isoforms mouse proteome database downloaded February 25, 2022 from Uniprot[91]. Walnut settings were: fixed cysteine carbamidomethylation, full tryptic digestion with up to 2 missed cleavages, HCD (y-only) fragmentation, 10 ppm precursor and fragment mass tolerances, and 5 quantitative ions. The chromatogram library resulting from the Walnut search was then used for Encyclopedia searching, where all similar settings to the Walnut search remained the same, and other settings included a library mass tolerance of 10 ppm, inclusion of both b- and y-type fragment ions, and a minimum number of quantitative ions set at 3. Percolator (version 3.1) was used to filter peptides to a 1% false discovery rate using the target/decoy approach and proteins to a 1% protein-level FDR assuming protein grouping parsimony. Resulting data from EncyclopeDIA were checked in Skyline[41] before further processing with Perseus[40]. Proteins were filtered so that only proteins with 2 or more peptides and those that were detected in all three replicates of at least one condition were retained. Data was converted to cell type-protein pairs, and the median value of the cell type-protein pair intensity was compared to the intensity of that protein detected in WT mice control samples. Keratins were manually removed from our dataset as these proteins are frequently detectable contaminants in mass spectrometry experiments[92]. To remove background labeling contaminants, only cell type-protein pairs that showed a greater than 1.5-fold intensity above the median intensity detected in WT samples were retained [32]. Then cell type-protein pairs with detected protein intensity across all 6 samples (sedentary and exercise) were included for downstream analysis. Next, cell type-protein pairs with variance > 2 ((log2(maximum intensity) − log2(minimum intensity)) > 2 under either sedentary or exercise conditions) were excluded from further analysis[93]. In total, 1272 cell type-protein pairs passed the above filtering criteria and were considered as bona fide cell type-protein pairs.

Exercise responsiveness scores calculations.—Exercise training-regulated cell type-protein pairs (adjusted P-values < 0.05 and exercise fold change > 1.5) were used for calculating exercise responsiveness scores. Each cell type-protein pair's exercise responsiveness was calculated as abs($\log_{10}$(adjusted P-values)) × abs($\log_2$(exercise fold change)). Exercise fold change of a cell type-protein pair was defined as median protein abundance across three exercise samples divided by median protein abundance across three sedentary samples of the same genotype. Then the exercise responsiveness scores were calculated by the summarization of the exercise responsiveness of each cell type-protein pair from the same cell type.

Time course of *Pdgfra*-cre secretomes.—AAV9-FLEx-ER-TurboID virus was injected as previously described into 6-week-old hemizygous male *Pdgfra*-creER mice at a dose of 3*10e11 GC per mouse. After a 2-week transduction period, tamoxifen was delivered to induce cre-mediated expression of ER-TurboID. Three weeks after the final tamoxifen injection, mice were divided into three groups (1-day running, 3-day running, 7-day running and sedentary controls, N = 3/condition). 1 h before the last bout of running, biotin was administered by injection (24 mg/ml, intraperitoneally, in a solution of 18:1:1 saline:Kolliphor EL:DMSO, final volume of 400 μl per mouse per day). The treadmill running was carried out as previously described. For the 1-day running group, mice were sacrificed, and blood and tissue samples were analyzed 2 h after a single bout of running. For 3-day or 7-day running groups, mice were run for 3 or 7 consecutive days and blood and tissues were harvested 2 h after the final bout of running. For the sedentary group, biotin was administered, and blood and tissue samples were collected 4 h after biotin delivery.

Gene ontology analysis.—Proteins with adjusted P-values < 0.05 and exercise fold change > 1.5 from *Pdgfra* secretomes were uploaded to online gene ontology analysis tool http://geneontology.org/ [94]. The enriched biological processes were ranked by gene ratio and P-values.

Isolation and culture of primary mouse hepatocytes.—Primary mouse hepatocytes were isolated and cultured as previously described[28,95]. Briefly, 8 to 12-week-old male mice (C57BL/6J) were sacrificed and perfused with perfusion buffer (1 g/L glucose, 2.1 g/L sodium bicarbonate, 0.4 g/L potassium chloride and 0.2 g/L EDTA in HBSS buffer) via cannulate vena cava for 5 to 8 min and then with digestion buffer (1 mg/ml collagenase IV (Sigma, C5138–1G) in DMEM/F-12 medium) for 5 to 8 min. The liver was then dissected out, cut into small pieces using a razor blade and passed through a 70-μm cell strainer (BD, 352350) to obtain crude hepatocytes. Cells were then spun down at 50 g for 3 min, resuspended in 10 ml plating medium (10% FBS, 1 μM dexamethasone (Sigma, D4902–100MG), 0.1 μM insulin (Sigma, 91077C), 2 mM sodium pyruvate, 1% penicillin–streptomycin in William's E medium (Quality Biological, 10128–636)) and spun down again at 50 g for additional 3 min. The pellet was resuspended in 10 ml of a 45% Percoll solution in PBS and spun down at 100 g for 10 min to isolate hepatocytes. The final hepatocyte pellet was resuspended in 10 ml plating medium, spun down again at 50 g for 5 min and resuspended in 1 ml plating medium. Cells were counted and plated in a collagen-coated six-well plate at 2 million cells per well. 4 h later, the plating medium was

changed to warm maintenance medium (0.1 μM dexamethasone, 1 nM insulin, 0.2% BSA (Sigma, A7906–500G), 2 mM sodium pyruvate, 1% penicillin–streptomycin), and cells were incubated overnight before further treatment.

Treatment of hepatocytes with organic compounds, MCT inhibitor and Brefeldin A.—24 h after plating, primary hepatocytes were washed twice with warm PBS to remove BSA. Then 2 ml William's E medium containing the indicated concentrations of sodium lactate (Sigma, 05508–5ML), 2 mM sodium fumarate dibasic (Sigma, F1506–25G), 2 mM sodium succinate dibasic hexahydrate (Sigma, S2378–100G), 2 mM sodium (R)-3-hydroxybutyrate (Sigma, 298360–1G), 2 mM kynurenic acid (Sigma, K3375–250MG), 2 mM D-Pantothenic acid hemicalcium salt (Sigma, 21210–5G-F), 2 mM sodium pyruvate (Sigma, P2256–25G), 2 mM L-(−)-Malic acid (Sigma, 02288–10G) was added. The above organic compounds powder was dissolved in ethyl alcohol 200 proof to make 100 mM master stock and diluted accordingly to reach the indicated concentration in medium. 40 μl ethanol was added as negative control. For MCT inhibitor AR-C155858 (Tocris, 4960) and Brefeldin A (Sigma, B6542–5MG), compound power was dissolved in DMSO to make master stock (100 μM for AR-C155858 and 5 mg/ml for Brefeldin A) and diluted accordingly to reach the indicated concentration in medium containing 2 mM sodium lactate. 4 h later, cells and conditioned medium were harvested and analyzed by western blotting as previously described. For HEK293T cells, cells were washed twice with warm PBS 24 h after transfection and incubated with serum-free medium containing indicated concentration of sodium lactate. 4 h later, cells and conditioned medium were harvested and analyzed by western blotting as described above.

Construction of plasmids for overexpression of CES2A/C-ΔC.—Flag-CES2A-ΔC fragment (ref sequence NM_133960.5) and Flag-CES2C-ΔC fragment (ref sequence NM_145603.2) were synthesized as gBlocks with IDT. For both fragments, 5'-GACTACAAGGATGACGACGATAAGGGGGGCGGT-3' sequences (encoding Flag tag) were inserted after CES2 sequences encoding secretory signal peptide (1–78 nt). For Flag-CES2A-ΔC fragment, C-terminal 5'-CATGCAGAGCTG-3' sequences (encoding HAEL as ER retention signal peptide) were deleted. For Flag-CES2C-ΔC fragment, C-terminal 5'-CACAGGGAGCTT-3' sequences (encoding HREL as ER retention signal peptide) were deleted. Both gene fragments were inserted into D-TOPO vector using pENTR/D-TOPO Cloning Kit (Invitrogen, K240020) and shuttled into pDEST40 mammalian expression vector using Gateway LR Clonase Enzyme mix (Invitrogen, 11791019). The pDEST40 plasmids were then transformed into One Shot TOP10 Chemically Competent E. coli (Invitrogen, C404010), extracted and sequence verified. pAAV-*Tbg*-ER-TurboID plasmid (Addgene, 149415) was cut with restriction enzymes NotI and HindIII to generate the backbone vector. Flag-CES2A-ΔC fragment was amplified using primer sets: 5'-TGCCTTTCTCTCCACAGGTGTCCAGGCGGCCGCGCCACCATGCCATTGGCTAGACTTC-3', 5'-CCAGAGGTTGATTGGATCCAAGCTTCTACTTGTCCTGAGAACCCTTGAGCTCCTG-3'. Flag-CES2C-ΔC fragment was amplified using primer sets: 5'-TGCCTTTCTCTCCACAGGTGTCCAGGCGGCCGCGCCACCATGACACGGAACCAACTACATAAC-3'; 5'-CCAGAGGT

TGATTGGATCCAAGCTTCTACTTGTCCTGAGAAGCCTTTAGCTCCTGG-3'. Both PCR products were purified using QIAquick gel extraction kit (Qiagen, 28704) and ligated with the linearized pAAV-*Tbg* vector using Gibson Assembly Master Mix (NEB Biolabs, E2611L). Ligated plasmids were transformed into One Shot TOP10 Chemically Competent E. coli (Invitrogen, C404010), extracted and sequence verified. pDEST40-Flag-CES2A-ΔC-S227A and pDEST40-Flag-CES2C-ΔC-S230A plasmids were generated with pDEST40-Flag-CES2A-ΔC and pDEST40-Flag-CES2C-ΔC as the templates respectively using Q5® Site-Directed Mutagenesis Kit (NEB Biolabs, E0554S). Flag-CES2A-ΔC-S227A and Flag-CES2C-ΔC-S230A fragments were amplified, purified and inserted into pAAV-*Tbg* vector as previously described.

Generation of recombinant CES2 proteins.—Recombinant CES2A and CES2C proteins were generated by transient transfection of pDEST40-CES2A/C-ΔC, pDEST40-CES2A-ΔC-S227A, pDEST40-CES2C-ΔC-S230A plasmids in mammalian Expi293 cells following the manufacturer's instructions. Five to seven days after transfection, conditioned medium was collected, and recombinant proteins were purified using a His GraviTrap TALON column and buffer exchanged to PBS. Protein purity and integrity were analyzed by SDS page. Following purification, recombinant proteins were aliquoted and stored at −80 °C to avoid freeze-thaws.

Determination of CES2A-ΔC and CES2C-ΔC secretion in cell culture.—HEK293T cells were transfected as described above. 30 h after transfection, cells were washed twice with PBS and added with 10 ml serum-free medium. 12 h later, conditioned medium (10 ml) was collected and concentrated 20-fold using 10 kDa filter tubes (Millipore, UFC801024) to 500 μl. Concentrated conditioned medium was mixed with 4× loading buffer (NuPAGE LDS Sample Buffer, Invitrogen, NP0008, 100 mM DTT) and boiled for 10 min at 95 °C. Cells were collected and lysed by probe sonication in RIPA buffer (1% NP-40, 0.1% SDS, 0.5% sodium deoxycholate and 1:100 HALT protease inhibitor, Thermo Fisher, 78429) for 1 min. Cell lysates were spun down at 13000 rpm for 10 min at 4 °C. The supernatant was collected, quantified using a tabletop Nanodrop One, boiled for 10 min at 95 °C. Both conditioned medium and cell lysate samples were then analyzed by western blot.

Histology.—Adipose tissues were collected into 4% paraformaldehyde and fixed at 4 °C with rotation for 72 h. Fixing solution was replaced with 20% sucrose solution. Adipose tissues were dehydrated for additional 24 h before freezing in OCT-embedded block (Thermo Fisher, 23–730-571) and cryosectioned. H&E staining was conducted on the slides by Stanford Animal Histology Core.

Glucose tolerance and insulin tolerance tests in mice.—For glucose tolerance tests, mice were fasted for 6 h (fasting starting 8 am in the morning) and then intraperitoneally injected with glucose at 2 g/kg body weight. Blood glucose levels were measured at 0, 20, 40, 60, and 120 mins via tail bleeding using a glucose meter. For insulin tolerance tests, mice were fasted for 6 h (fasting starting 8 am in the morning) and then intraperitoneally injected with insulin in saline 0.75 U/kg body weight. Blood glucose levels were measured at 0, 20, 40, 60, and 120 mins via tail bleeding using a glucose meter.

Maximal running capacity test.—8 weeks after viral transduction, mice were acclimated to the treadmill two days prior to the maximal running tests (10 min at 10 m/min). The maximal running test was performed as previously described[70,85]. Briefly, running started at 9.6 m/min with 14.5° incline for 60 s, followed by a continuous increase (1.2 m/min) in running speed every 60 s until exhaustion. The test was randomized where each experimental group ran on different lanes of the treadmill. In addition, the test was also performed blinded (one person placing the mice on the treadmills, another person (blinded) to determine the exhaustion of the individual mouse).

Chronic treadmill running.—8 to 10-week-old male C57BL/6 mice were injected with AAV8-*Tbg*- CES2A/C-ΔC/GFP viruses via tail vein at a dose of 10e11 GC per mouse. One week after viral transduction, mice were fed with HFD (60% fat, Research Diets, D12492) for 4-weeks. Then mice Body weights and food intake were measured every week. Starting from the 5^{th} week, mice were subjected to treadmill running daily (5 day per week) for 4 consecutive weeks. Mice were acclimated to the treadmill for 5 minutes before running at a speed of 5 m/min for 5 min. Then the speed was increased to 15 m/min and kept constant for 60 min. A serological pipette was used to manually stir the mice to avoid excessive electrical shock during the whole running period. After exercise training, mice were returned to home cages. The sedentary control animals were kept in their home cages but removed from the original racks and put next to the treadmill. These mice were constantly disturbed by the noises from the running animals and treadmill and therefore were kept awake during the whole duration of the running of the exercise animals. Running was performed for 5 consecutive days in the morning (between 9–12 am) per week followed by 2-day rest.

Indirect calorimetry and physiological measurements.—8 to 10-week-old male C57BL/6 mice were injected with AAV8-*Tbg*- CES2A/C-ΔC/GFP viruses via tail vein at a dose of 10^{11} GC per mouse. One week after viral transduction, mice were fed with HFD (60% fat, Research Diets, D12492). Body weights and food intake were measured every week. Before the body weights of AAV8-*Tbg*-CES2A/C-ΔC injected mice started to be significantly different from AAV8-*Tbg*-GFP injected mice (~3 week for AAV8-*Tbg*-CES2C-ΔC and ~5 week for AAV8-*Tbg*-CES2A-ΔC), metabolic parameters including oxygen consumption, respiratory exchange ratio, food intake and movement of mice were measured using the environment-controlled home-cage CLAMS system (Columbus Instruments) at the Stanford Diabetes Center. Mice were housed in the metabolic chambers for 24 h prior to the start of experiment. Energy expenditure calculations were normalized for body weight. P-values were calculated from two-way ANOVA.

LC-MS detection of blood plasma lactate.—10 to 12-week old male C57BL/6 mice were subjected to 1-week treadmill running protocol used in this experiment. The sedentary control animals were kept in their home cages but removed from the original racks and put next to the treadmill. These mice were constantly disturbed by the noises from the running animals and treadmill and therefore were kept awake during the whole duration of the running of the exercise animals. The exercise mice were sacrificed immediately after the last bout of running and blood plasma was harvested and processed as previously described. Then 150 μl of a 2:1 mixture of acetonitrile:methanol was added to 50 μl of

plasma to extract polar metabolites. The mixture was then spun down at 13,000 rpm for 10 min at 4 °C and the supernatant was transferred to a LC–MS vial for analysis using an Agilent 6470 triple quadrupole LC–MS instrument. Separation of polar metabolites was conducted as previously described (Lac-phe paper). Briefly, a Luna 5 μm NH2 100 Å LC column (Phenomenex 00B-4378-E0) was used for LC with normal phase chromatography. Mobile phases compositions were as follows: buffer A, 95:5 water:acetonitrile with 0.2% ammonium hydroxide and 10 mM ammonium acetate; buffer B, acetonitrile. The LC gradient started at 100% buffer B with a flow rate of 0.7 ml/min from 0 to 2 min. The gradient was then linearly increased to 50% A/50% B at a flow rate of 0.7 ml/min from 2 to 20 min. From 20 to 25 min, the gradient was maintained at 50% A/50% B at a flow rate of 0.7 ml/min. Finally, 100% buffer B was maintained at a flow rate of 0.7 ml/min for 5min to equilibrate the column. MS analysis was performed in negative mode using ESI. The AJS ESI source parameters were set as follows: the capillary voltage was set to 3,500 V; the sheath gas temperature was set to 300 °C with the sheath gas flow set at 12 l/min; and the gas temperature was set at 250 °C with a gas flow of 12 l/min and the nebulizer pressure was at 25 psi. Quantification of the plasma lactate concentrations were performed by generating a standard curve with known concentrations of sodium lactate. Lactate standards were analyzed using the same targeted method and run on the same batch and a standard curve was generated from the lactate concentrations and total ion intensities were used to calculate the plasma lactate concentrations.

Untargeted metabolomics by LC-MS.—12 to 16-week old male C57BL/6 mice (N = 5/group) transduced with AAV-*Tbg*-CES2A-ΔC, AAV-*Tbg*-CES2C-ΔC or AAV-*Tbg*-GFP Untargeted metabolomics measurements were then performed as previously described[96]. Briefly, an Agilent 6520 Quadrupole time-of-flight LC–MS instrument was used for analysis. MS runs were performed using electrospray ionization (ESI) in negative mode. The dual ESI source parameters were set as follows: the gas temperature was set at 250 °C with a drying gas flow of 12 l/min and the nebulizer pressure at 20 psi; the capillary voltage was set to 3,500 V; and the fragmentor voltage was set to 100 V. A Luna 5 μm NH2 100 Å LC column (Phenomenex 00B-4378-E0) with normal phase chromatography was used to separate polar metabolites. Mobile phases and LC parameters were the same as the lactate quantification LC-MS runs described above. Differential peak identification was performed with XCMS[97].

Carboxylesterases enzymatic activity measurement.—A continuous spectrophotometric assay was performed using 4-nitrophenyl acetate (Sigma, N8130–5G) as substrate as previously described [98]. Briefly, 1 mM 4-nitrophenyl acetate was prepared freshly in 50 mM Tris·Cl buffer (pH 7.4). 150 μl of 4-nitrophenyl acetate solution was added into a single well of a 96-well plate (Thermo Fisher, 125565501), followed by pre-incubating 5 min at 37 °C in the absorbance plate reader. 15 μg liver lysates or 3 μl plasma were diluted in 50 mM Tris·Cl buffer (pH 7.4) and added to 4-nitrophenyl acetate solution (total volume 300 μl). The formation of p-nitrophenolate was measured every 30 s at 405 nm for 5 min. Subtracted from background absorbance, absorbance at each time point was used to generate a kinetic plot for each sample. Data points within the linear range

of the reaction were used to calculate the slope of the enzymatic reaction. Finally, relative enzymatic activity was calculated comparing the slopes of reaction from each sample.

Quantification and statistical analysis

Data representation and statistical analysis.—All values in figures are shown as mean ± SEM. The number of biological replicates (N) is described in each figure legend (N corresponds to the number of animals used under each condition for animal experiments and corresponds to the number of independently conducted experiments for cellular experiments). For animal studies, mice were randomly assigned to control and treatment groups. Each animal study was repeated at least twice using separate cohorts of mice. To identify statistically changed cell type-protein pairs (exercise vs sedentary, N = 3/protein/condition/genotype), protein intensities were first scaled by the scale() function in R package[99]. The Limma package[100,101] was implemented to conduct the moderated t-statistics[102] (https://github.com/leolove2022/ModeratedtTest.git), and adjusted P-values of each cell type-protein pair were generated into excel files. 256 cell type-protein pairs out of total 1272 pairs were defined as under exercise training regulation (adjusted P-values < 0.05 and exercise fold change > 1.5). Each in vitro experiment using primary cells from mice was repeated using at least three cohorts of mice. Two-tailed, unpaired student's t-test was used for single comparisons assuming the sample groups exhibited a normal distribution and comparable variance. Two-way ANOVA with post hoc Sidak's multiple comparisons test with repeated measures was used for the body weights, glucose tolerance test and insulin tolerance test studies. Unless otherwise specified, statistical significance was set at adjusted P-value < 0.05 for the proteomics data, and P-value < 0.05 for all other comparisons.

Supplementary Material

Refer to Web version on PubMed Central for supplementary material.

Acknowledgment

We thank members of the Long, Bertozzi and Svensson labs for helpful discussions. We gratefully acknowledge the staff at the Penn Vector Core (RRID: SCR_022432) for the production of AAVs. This work was supported by the US National Institutes of Health (DK105203 and DK124265 to J.Z.L, DK125260 and DK111916 to K.J.S, K99GM147304 to N.M.R.), the Wu Tsai Human Performance Alliance (research grant to J.Z.L, postdoctoral fellowship to X.C.), the Stanford Diabetes Research Center (P30DK116074), the Stanford Cardiovascular institute (CVI), the Weintz Family COVID-19 research fund (K.J.S), American Heart Association (AHA), the Stanford School of Medicine, the Jacob Churg Foundation (K.J.S), the McCormick and Gabilan Award (K.J.S), Vanessa Kong-Kerzner foundation (graduate fellowship to W.W.), the American Heart Association (postdoctoral fellowship to M.Z.), Fundacion Alfonso Martin Escudero (postdoctoral fellowship to M.D.M.G.), and Independent Research Fund Denmark (2030-00007A) and the Lundbeck Foundation (R380-2021-1451) (S.H.R).

References

1. Piercy KL, Troiano RP, Ballard RM, Carlson SA, Fulton JE, Galuska DA, George SM, and Olson RD (2018). The Physical Activity Guidelines for Americans. JAMA 320, 2020–2028. 10.1001/jama.2018.14854. [PubMed: 30418471]
2. Warburton DER, and Bredin SSD (2017). Health benefits of physical activity: a systematic review of current systematic reviews. Curr Opin Cardiol 32, 541–556. 10.1097/HCO.0000000000000437. [PubMed: 28708630]
3. Lear SA, Hu W, Rangarajan S, Gasevic D, Leong D, Iqbal R, Casanova A, Swaminathan S, Anjana RM, Kumar R, et al. (2017). The effect of physical activity on mortality and cardiovascular disease

in 130 000 people from 17 high-income, middle-income, and low-income countries: the PURE study. Lancet 390, 2643–2654. 10.1016/S0140-6736(17)31634-3. [PubMed: 28943267]

4. Booth FW, Roberts CK, Thyfault JP, Ruegsegger GN, and Toedebusch RG (2017). Role of Inactivity in Chronic Diseases: Evolutionary Insight and Pathophysiological Mechanisms. Physiol Rev 97, 1351–1402. 10.1152/physrev.00019.2016. [PubMed: 28814614]
5. Knowler WC, Barrett-Connor E, Fowler SE, Hamman RF, Lachin JM, Walker EA, Nathan DM, and Group DPPR (2002). Reduction in the incidence of type 2 diabetes with lifestyle intervention or metformin. N Engl J Med 346, 393–403. 10.1056/NEJMoa012512. [PubMed: 11832527]
6. Hambrecht R, Walther C, Möbius-Winkler S, Gielen S, Linke A, Conradi K, Erbs S, Kluge R, Kendziorra K, Sabri O, et al. (2004). Percutaneous coronary angioplasty compared with exercise training in patients with stable coronary artery disease: a randomized trial. Circulation 109, 1371–1378. 10.1161/01.CIR.0000121360.31954.1F. [PubMed: 15007010]
7. Blair SN, Kohl HW, Paffenbarger RS, Clark DG, Cooper KH, and Gibbons LW (1989). Physical fitness and all-cause mortality. A prospective study of healthy men and women. JAMA 262, 2395–2401. 10.1001/jama.262.17.2395. [PubMed: 2795824]
8. Neufer PD, Bamman MM, Muoio DM, Bouchard C, Cooper DM, Goodpaster BH, Booth FW, Kohrt WM, Gerszten RE, Mattson MP, et al. (2015). Understanding the Cellular and Molecular Mechanisms of Physical Activity-Induced Health Benefits. Cell Metab 22, 4–11. 10.1016/j.cmet.2015.05.011. [PubMed: 26073496]
9. McGee SL, and Hargreaves M (2020). Exercise adaptations: molecular mechanisms and potential targets for therapeutic benefit. Nat Rev Endocrinol 16, 495–505. 10.1038/s41574-020-0377-1. [PubMed: 32632275]
10. Chow LS, Gerszten RE, Taylor JM, Pedersen BK, van Praag H, Trappe S, Febbraio MA, Galis ZS, Gao Y, Haus JM, et al. (2022). Exerkines in health, resilience and disease. Nat Rev Endocrinol 18, 273–289. 10.1038/s41574-022-00641-2. [PubMed: 35304603]
11. Safdar A, Saleem A, and Tarnopolsky MA (2016). The potential of endurance exercise-derived exosomes to treat metabolic diseases. Nat Rev Endocrinol 12, 504–517. 10.1038/nrendo.2016.76. [PubMed: 27230949]
12. Goldstein MS (1961). Humoral Nature of the Hypoglycemic Factor of Muscular Work. Diabetes 10, 232–234. 10.2337/diab.10.3.232. [PubMed: 13706674]
13. Horowitz AM, Fan X, Bieri G, Smith LK, Sanchez-Diaz CI, Schroer AB, Gontier G, Casaletto KB, Kramer JH, Williams KE, and Villeda SA (2020). Blood factors transfer beneficial effects of exercise on neurogenesis and cognition to the aged brain. Science 369, 167–173. 10.1126/science.aaw2622. [PubMed: 32646997]
14. De Miguel Z, Khoury N, Betley MJ, Lehallier B, Willoughby D, Olsson N, Yang AC, Hahn O, Lu N, Vest RT, et al. (2021). Exercise plasma boosts memory and dampens brain inflammation via clusterin. Nature 600, 494–499. 10.1038/s41586-021-04183-x. [PubMed: 34880498]
15. Steensberg A, van Hall G, Osada T, Sacchetti M, Saltin B, and Klarlund Pedersen B (2000). Production of interleukin-6 in contracting human skeletal muscles can account for the exercise-induced increase in plasma interleukin-6. J Physiol 529 Pt 1, 237–242. 10.1111/j.1469-7793.2000.00237.x. [PubMed: 11080265]
16. Knudsen NH, Stanya KJ, Hyde AL, Chalom MM, Alexander RK, Liou YH, Starost KA, Gangl MR, Jacobi D, Liu S, et al. (2020). Interleukin-13 drives metabolic conditioning of muscle to endurance exercise. Science 368. 10.1126/science.aat3987.
17. Boström P, Wu J, Jedrychowski MP, Korde A, Ye L, Lo JC, Rasbach KA, Boström EA, Choi JH, Long JZ, et al. (2012). A PGC1-α-dependent myokine that drives brown-fat-like development of white fat and thermogenesis. Nature 481, 463–468. 10.1038/nature10777. [PubMed: 22237023]
18. Wrann CD, White JP, Salogiannnis J, Laznik-Bogoslavski D, Wu J, Ma D, Lin JD, Greenberg ME, and Spiegelman BM (2013). Exercise induces hippocampal BDNF through a PGC-1α/FNDC5 pathway. Cell Metab 18, 649–659. 10.1016/j.cmet.2013.09.008. [PubMed: 24120943]
19. Rao RR, Long JZ, White JP, Svensson KJ, Lou J, Lokurkar I, Jedrychowski MP, Ruas JL, Wrann CD, Lo JC, et al. (2014). Meteorin-like is a hormone that regulates immune-adipose interactions to increase beige fat thermogenesis. Cell 157, 1279–1291. 10.1016/j.cell.2014.03.065. [PubMed: 24906147]

20. Reddy A, Bozi LHM, Yaghi OK, Mills EL, Xiao H, Nicholson HE, Paschini M, Paulo JA, Garrity R, Laznik-Bogoslavski D, et al. (2020). pH-Gated Succinate Secretion Regulates Muscle Remodeling in Response to Exercise. Cell 183, 62–75.e17. 10.1016/j.cell.2020.08.039. [PubMed: 32946811]
21. Agudelo LZ, Femenía T, Orhan F, Porsmyr-Palmertz M, Goiny M, Martinez-Redondo V, Correia JC, Izadi M, Bhat M, Schuppe-Koistinen I, et al. (2014). Skeletal muscle PGC-1α1 modulates kynurenine metabolism and mediates resilience to stress-induced depression. Cell 159, 33–45. 10.1016/j.cell.2014.07.051. [PubMed: 25259918]
22. Sato S, Dyar KA, Treebak JT, Jepsen SL, Ehrlich AM, Ashcroft SP, Trost K, Kunzke T, Prade VM, Small L, et al. (2022). Atlas of exercise metabolism reveals time-dependent signatures of metabolic homeostasis. Cell Metab 34, 329–345.e328. 10.1016/j.cmet.2021.12.016. [PubMed: 35030324]
23. Takahashi H, Alves CRR, Stanford KI, Middelbeek RJW, Nigro P, Ryan RE, Xue R, Sakaguchi M, Lynes MD, So K, et al. (2019). TGF-β2 is an exercise-induced adipokine that regulates glucose and fatty acid metabolism. Nat Metab 1, 291–303. 10.1038/s42255-018-0030-7. [PubMed: 31032475]
24. Lynes MD, Leiria LO, Lundh M, Bartelt A, Shamsi F, Huang TL, Takahashi H, Hirshman MF, Schlein C, Lee A, et al. (2017). The cold-induced lipokine 12,13-diHOME promotes fatty acid transport into brown adipose tissue. Nat Med 23, 631–637. 10.1038/nm.4297. [PubMed: 28346411]
25. Uhlén M, Fagerberg L, Hallström BM, Lindskog C, Oksvold P, Mardinoglu A, Sivertsson Å, Kampf C, Sjöstedt E, Asplund A, et al. (2015). Proteomics. Tissue-based map of the human proteome. Science 347, 1260419. 10.1126/science.1260419. [PubMed: 25613900]
26. Somineni HK, Boivin GP, and Elased KM (2014). Daily exercise training protects against albuminuria and angiotensin converting enzyme 2 shedding in db/db diabetic mice. J Endocrinol 221, 235–251. 10.1530/JOE-13-0532. [PubMed: 24756098]
27. Wei W, Riley NM, Lyu X, Bertozzi CR, and Long JZ (2021). Protocol for cell type-specific labeling, enrichment, and proteomic profiling of plasma proteins in mice. STAR Protoc 2, 101014. 10.1016/j.xpro.2021.101014. [PubMed: 34950890]
28. Wei W, Riley NM, Yang AC, Kim JT, Terrell SM, Li VL, Garcia-Contreras M, Bertozzi CR, and Long JZ (2020). Cell type-selective secretome profiling in vivo. Nat Chem Biol. 10.1038/s41589-020-00698-y.
29. Droujinine IA, Meyer AS, Wang D, Udeshi ND, Hu Y, Rocco D, McMahon JA, Yang R, Guo J, Mu L, et al. (2021). Proteomics of protein trafficking by in vivo tissue-specific labeling. Nat Commun 12, 2382. 10.1038/s41467-021-22599-x. [PubMed: 33888706]
30. Kim KE, Park I, Kim J, Kang MG, Choi WG, Shin H, Kim JS, Rhee HW, and Suh JM (2021). Dynamic tracking and identification of tissue-specific secretory proteins in the circulation of live mice. Nat Commun 12, 5204. 10.1038/s41467-021-25546-y. [PubMed: 34471136]
31. Liu J, Jang JY, Pirooznia M, Liu S, and Finkel T (2021). The secretome mouse provides a genetic platform to delineate tissue-specific in vivo secretion. Proc Natl Acad Sci U S A 118. 10.1073/pnas.2005134118.
32. Branon TC, Bosch JA, Sanchez AD, Udeshi ND, Svinkina T, Carr SA, Feldman JL, Perrimon N, and Ting AY (2018). Efficient proximity labeling in living cells and organisms with TurboID. Nat Biotechnol 36, 880–887. 10.1038/nbt.4201. [PubMed: 30125270]
33. Zincarelli C, Soltys S, Rengo G, and Rabinowitz JE (2008). Analysis of AAV serotypes 1–9 mediated gene expression and tropism in mice after systemic injection. Mol Ther 16, 1073–1080. 10.1038/mt.2008.76. [PubMed: 18414476]
34. Wu J, Ruas JL, Estall JL, Rasbach KA, Choi JH, Ye L, Boström P, Tyra HM, Crawford RW, Campbell KP, et al. (2011). The unfolded protein response mediates adaptation to exercise in skeletal muscle through a PGC-1α/ATF6α complex. Cell Metab 13, 160–169. 10.1016/j.cmet.2011.01.003. [PubMed: 21284983]
35. Finck BN, and Kelly DP (2006). PGC-1 coactivators: inducible regulators of energy metabolism in health and disease. J Clin Invest 116, 615–622. 10.1172/JCI27794. [PubMed: 16511594]

36. Kawasaki E, Hokari F, Sasaki M, Sakai A, Koshinaka K, and Kawanaka K (2009). Role of local muscle contractile activity in the exercise-induced increase in NR4A receptor mRNA expression. J Appl Physiol (1985) 106, 1826–1831. 10.1152/japplphysiol.90923.2008. [PubMed: 19359610]
37. Lewis GD, Farrell L, Wood MJ, Martinovic M, Arany Z, Rowe GC, Souza A, Cheng S, McCabe EL, Yang E, et al. (2010). Metabolic signatures of exercise in human plasma. Sci Transl Med 2, 33ra37. 10.1126/scitranslmed.3001006.
38. Searle BC, Pino LK, Egertson JD, Ting YS, Lawrence RT, MacLean BX, Villén J, and MacCoss MJ (2018). Chromatogram libraries improve peptide detection and quantification by data independent acquisition mass spectrometry. Nat Commun 9, 5128. 10.1038/s41467-018-07454-w. [PubMed: 30510204]
39. Pino LK, Just SC, MacCoss MJ, and Searle BC (2020). Acquiring and Analyzing Data Independent Acquisition Proteomics Experiments without Spectrum Libraries. Mol Cell Proteomics 19, 1088–1103. 10.1074/mcp.P119.001913. [PubMed: 32312845]
40. Tyanova S, Temu T, Sinitcyn P, Carlson A, Hein MY, Geiger T, Mann M, and Cox J (2016). The Perseus computational platform for comprehensive analysis of (prote)omics data. Nat Methods 13, 731–740. 10.1038/nmeth.3901. [PubMed: 27348712]
41. Pino LK, Searle BC, Bollinger JG, Nunn B, MacLean B, and MacCoss MJ (2020). The Skyline ecosystem: Informatics for quantitative mass spectrometry proteomics. Mass Spectrom Rev 39, 229–244. 10.1002/mas.21540. [PubMed: 28691345]
42. Stern JH, Rutkowski JM, and Scherer PE (2016). Adiponectin, Leptin, and Fatty Acids in the Maintenance of Metabolic Homeostasis through Adipose Tissue Crosstalk. Cell Metab 23, 770–784. 10.1016/j.cmet.2016.04.011. [PubMed: 27166942]
43. Liu H, Chen SE, Jin B, Carson JA, Niu A, Durham W, Lai JY, and Li YP (2010). TIMP3: a physiological regulator of adult myogenesis. J Cell Sci 123, 2914–2921. 10.1242/jcs.057620. [PubMed: 20682640]
44. Hanaoka Y, Yasuda O, Soejima H, Miyata K, Yamamoto E, Izumiya Y, Maeda N, Ohishi M, Rakugi H, Oike Y, et al. (2014). Tissue inhibitor of metalloproteinase-3 knockout mice exhibit enhanced energy expenditure through thermogenesis. PLoS One 9, e94930. 10.1371/journal.pone.0094930. [PubMed: 24736588]
45. Basu R, Lee J, Morton JS, Takawale A, Fan D, Kandalam V, Wang X, Davidge ST, and Kassiri Z (2013). TIMP3 is the primary TIMP to regulate agonist-induced vascular remodelling and hypertension. Cardiovasc Res 98, 360–371. 10.1093/cvr/cvt067. [PubMed: 23524300]
46. Stöhr R, Cavalera M, Menini S, Mavilio M, Casagrande V, Rossi C, Urbani A, Cardellini M, Pugliese G, Menghini R, and Federici M (2014). Loss of TIMP3 exacerbates atherosclerosis in ApoE null mice. Atherosclerosis 235, 438–443. 10.1016/j.atherosclerosis.2014.05.946. [PubMed: 24943223]
47. Abdelsaid K, Sudhahar V, Harris RA, Das A, Youn SW, Liu Y, McMenamin M, Hou Y, Fulton D, Hamrick MW, et al. (2022). Exercise improves angiogenic function of circulating exosomes in type 2 diabetes: Role of exosomal SOD3. FASEB J 36, e22177. 10.1096/fj.202101323R. [PubMed: 35142393]
48. Hitomi Y, Watanabe S, Kizaki T, Sakurai T, Takemasa T, Haga S, Ookawara T, Suzuki K, and Ohno H (2008). Acute exercise increases expression of extracellular superoxide dismutase in skeletal muscle and the aorta. Redox Rep 13, 213–216. 10.1179/135100008X308894. [PubMed: 18796240]
49. Fukai T, Siegfried MR, Ushio-Fukai M, Cheng Y, Kojda G, and Harrison DG (2000). Regulation of the vascular extracellular superoxide dismutase by nitric oxide and exercise training. J Clin Invest 105, 1631–1639. 10.1172/JCI9551. [PubMed: 10841522]
50. Kusuyama J, Alves-Wagner AB, Conlin RH, Makarewicz NS, Albertson BG, Prince NB, Kobayashi S, Kozuka C, Møller M, Bjerre M, et al. (2021). Placental superoxide dismutase 3 mediates benefits of maternal exercise on offspring health. Cell Metab 33, 939–956.e938. 10.1016/j.cmet.2021.03.004. [PubMed: 33770509]
51. Raschke S, Eckardt K, Bjørklund Holven K, Jensen J, and Eckel J (2013). Identification and validation of novel contraction-regulated myokines released from primary human skeletal muscle cells. PLoS One 8, e62008. 10.1371/journal.pone.0062008. [PubMed: 23637948]

52. Duggan C, Xiao L, Wang CY, and McTiernan A (2014). Effect of a 12-month exercise intervention on serum biomarkers of angiogenesis in postmenopausal women: a randomized controlled trial. Cancer Epidemiol Biomarkers Prev 23, 648–657. 10.1158/1055-9965.EPI-13-1155. [PubMed: 24501378]

53. Zepp JA, Zacharias WJ, Frank DB, Cavanaugh CA, Zhou S, Morley MP, and Morrisey EE (2017). Distinct Mesenchymal Lineages and Niches Promote Epithelial Self-Renewal and Myofibrogenesis in the Lung. Cell 170, 1134–1148.e1110. 10.1016/j.cell.2017.07.034. [PubMed: 28886382]

54. Li R, Bernau K, Sandbo N, Gu J, Preissl S, and Sun X (2018). marks a cellular lineage with distinct contributions to myofibroblasts in lung maturation and injury response. Elife 7. 10.7554/eLife.36865.

55. Merrick D, Sakers A, Irgebay Z, Okada C, Calvert C, Morley MP, Percec I, and Seale P (2019). Identification of a mesenchymal progenitor cell hierarchy in adipose tissue. Science 364. 10.1126/science.aav2501.

56. Schranner D, Kastenmuller G, Schonfelder M, Romisch-Margl W, and Wackerhage H (2020). Metabolite Concentration Changes in Humans After a Bout of Exercise: a Systematic Review of Exercise Metabolomics Studies. Sports Med Open 6, 11. 10.1186/s40798-020-0238-4. [PubMed: 32040782]

57. Contrepois K, Wu S, Moneghetti KJ, Hornburg D, Ahadi S, Tsai MS, Metwally AA, Wei E, Lee-McMullen B, Quijada JV, et al. (2020). Molecular Choreography of Acute Exercise. Cell 181, 1112–1130.e1116. 10.1016/j.cell.2020.04.043. [PubMed: 32470399]

58. Ovens MJ, Davies AJ, Wilson MC, Murray CM, and Halestrap AP (2010). AR-C155858 is a potent inhibitor of monocarboxylate transporters MCT1 and MCT2 that binds to an intracellular site involving transmembrane helices 7–10. Biochem J 425, 523–530. 10.1042/BJ20091515. [PubMed: 19929853]

59. Ovens MJ, Manoharan C, Wilson MC, Murray CM, and Halestrap AP (2010). The inhibition of monocarboxylate transporter 2 (MCT2) by AR-C155858 is modulated by the associated ancillary protein. Biochem J 431, 217–225. 10.1042/BJ20100890. [PubMed: 20695846]

60. Xu Y, Pan X, Hu S, Zhu Y, Cassim Bawa F, Li Y, Yin L, and Zhang Y (2021). Hepatocyte-specific expression of human carboxylesterase 2 attenuates nonalcoholic steatohepatitis in mice. Am J Physiol Gastrointest Liver Physiol 320, G166–G174. 10.1152/ajpgi.00315.2020. [PubMed: 33325808]

61. Li Y, Zalzala M, Jadhav K, Xu Y, Kasumov T, Yin L, and Zhang Y (2016). Carboxylesterase 2 prevents liver steatosis by modulating lipolysis, endoplasmic reticulum stress, and lipogenesis and is regulated by hepatocyte nuclear factor 4 alpha in mice. Hepatology 63, 1860–1874. 10.1002/hep.28472. [PubMed: 26806650]

62. Ruby MA, Massart J, Hunerdosse DM, Schonke M, Correia JC, Louie SM, Ruas JL, Naslund E, Nomura DK, and Zierath JR (2017). Human Carboxylesterase 2 Reverses Obesity-Induced Diacylglycerol Accumulation and Glucose Intolerance. Cell Rep 18, 636–646. 10.1016/j.celrep.2016.12.070. [PubMed: 28099843]

63. Maresch LK, Benedikt P, Feiler U, Eder S, Zierler KA, Taschler U, Kolleritsch S, Eichmann TO, Schoiswohl G, Leopold C, et al. (2019). Intestine-Specific Overexpression of Carboxylesterase 2c Protects Mice From Diet-Induced Liver Steatosis and Obesity. Hepatol Commun 3, 227–245. 10.1002/hep4.1292. [PubMed: 30766961]

64. Hsieh YT, Lin HP, Chen BM, Huang PT, and Roffler SR (2015). Effect of Cellular Location of Human Carboxylesterase 2 on CPT-11 Hydrolysis and Anticancer Activity. PLoS One 10, e0141088. 10.1371/journal.pone.0141088. [PubMed: 26509550]

65. Oosterhoff D, Overmeer RM, de Graaf M, van der Meulen IH, Giaccone G, van Beusechem VW, Haisma HJ, Pinedo HM, and Gerritsen WR (2005). Adenoviral vector-mediated expression of a gene encoding secreted, EpCAM-targeted carboxylesterase-2 sensitises colon cancer spheroids to CPT-11. Br J Cancer 92, 882–887. 10.1038/sj.bjc.6602362. [PubMed: 15756257]

66. Potter PM, Wolverton JS, Morton CL, Wierdl M, and Danks MK (1998). Cellular localization domains of a rabbit and a human carboxylesterase: influence on irinotecan (CPT-11) metabolism by the rabbit enzyme. Cancer Res 58, 3627–3632. [PubMed: 9721871]

67. Wei W, Riley NM, Yang AC, Kim JT, Terrell SM, Li VL, Garcia-Contreras M, Bertozzi CR, and Long JZ (2021). Cell type-selective secretome profiling in vivo. Nat Chem Biol 17, 326–334. 10.1038/s41589-020-00698-y. [PubMed: 33199915]
68. Raven A, Lu WY, Man TY, Ferreira-Gonzalez S, O'Duibhir E, Dwyer BJ, Thomson JP, Meehan RR, Bogorad R, Koteliansky V, et al. (2017). Cholangiocytes act as facultative liver stem cells during impaired hepatocyte regeneration. Nature 547, 350–354. 10.1038/nature23015. [PubMed: 28700576]
69. Wang G, Chow RD, Ye L, Guzman CD, Dai X, Dong MB, Zhang F, Sharp PA, Platt RJ, and Chen S (2018). Mapping a functional cancer genome atlas of tumor suppressors in mouse liver using AAV-CRISPR-mediated direct in vivo screening. Sci Adv 4, eaao5508. 10.1126/sciadv.aao5508. [PubMed: 29503867]
70. Raun SH, Henriquez-Olguin C, Karavaeva I, Ali M, Moller LLV, Kot W, Castro-Mejia JL, Nielsen DS, Gerhart-Hines Z, Richter EA, and Sylow L (2020). Housing temperature influences exercise training adaptations in mice. Nat Commun 11, 1560. 10.1038/s41467-020-15311-y. [PubMed: 32214091]
71. Møller LLV, Raun SH, Fritzen AM, and Sylow L (2022). Measurement of skeletal muscle glucose uptake in mice in response to acute treadmill running. J Biol Methods 9, e162. 10.14440/jbm.2022.385. [PubMed: 36404875]
72. Guijas C, Montenegro-Burke JR, Domingo-Almenara X, Palermo A, Warth B, Hermann G, Koellensperger G, Huan T, Uritboonthai W, Aisporna AE, et al. (2018). METLIN: A Technology Platform for Identifying Knowns and Unknowns. Anal Chem 90, 3156–3164. 10.1021/acs.analchem.7b04424. [PubMed: 29381867]
73. De Nardo W, Miotto PM, Bayliss J, Nie S, Keenan SN, Montgomery MK, and Watt MJ (2022). Proteomic analysis reveals exercise training induced remodelling of hepatokine secretion and uncovers syndecan-4 as a regulator of hepatic lipid metabolism. Mol Metab 60, 101491. 10.1016/j.molmet.2022.101491. [PubMed: 35381388]
74. Yang J, Vamvini M, Nigro P, Ho LL, Galani K, Alvarez M, Tanigawa Y, Renfro A, Carbone NP, Laakso M, et al. (2022). Single-cell dissection of the obesity-exercise axis in adipose-muscle tissues implies a critical role for mesenchymal stem cells. Cell Metab 34, 1578–1593.e1576. 10.1016/j.cmet.2022.09.004. [PubMed: 36198295]
75. Shin S, Pang Y, Park J, Liu L, Lukas BE, Kim SH, Kim KW, Xu P, Berry DC, and Jiang Y (2020). Dynamic control of adipose tissue development and adult tissue homeostasis by platelet-derived growth factor receptor alpha. Elife 9. 10.7554/eLife.56189.
76. Guseh JS, Churchill TW, Yeri A, Lo C, Brown M, Houstis NE, Aragam KG, Lieberman DE, Rosenzweig A, and Baggish AL (2020). An expanded repertoire of intensity-dependent exercise-responsive plasma proteins tied to loci of human disease risk. Sci Rep 10, 10831. 10.1038/s41598-020-67669-0. [PubMed: 32616758]
77. Tang S, Beattie AT, Kafkova L, Petris G, Huguenin-Dezot N, Fiedler M, Freeman M, and Chin JW (2022). Mechanism-based traps enable protease and hydrolase substrate discovery. Nature 602, 701–707. 10.1038/s41586-022-04414-9. [PubMed: 35173328]
78. Sato S, Basse AL, Schönke M, Chen S, Samad M, Altıntaş A, Laker RC, Dalbram E, Barrès R, Baldi P, et al. (2019). Time of Exercise Specifies the Impact on Muscle Metabolic Pathways and Systemic Energy Homeostasis. Cell Metab 30, 92–110.e114. 10.1016/j.cmet.2019.03.013. [PubMed: 31006592]
79. Ezagouri S, Zwighaft Z, Sobel J, Baillieul S, Doutreleau S, Ladeuix B, Golik M, Verges S, and Asher G (2019). Physiological and Molecular Dissection of Daily Variance in Exercise Capacity. Cell Metab 30, 78–91.e74. 10.1016/j.cmet.2019.03.012. [PubMed: 31006590]
80. Pendergrast LA, Lundell LS, Ehrlich AM, Ashcroft SP, Schönke M, Basse AL, Krook A, Treebak JT, Dollet L, and Zierath JR (2023). Time of day determines postexercise metabolism in mouse adipose tissue. Proc Natl Acad Sci U S A 120, e2218510120. 10.1073/pnas.2218510120. [PubMed: 36780527]
81. Wilkinson SB, Phillips SM, Atherton PJ, Patel R, Yarasheski KE, Tarnopolsky MA, and Rennie MJ (2008). Differential effects of resistance and endurance exercise in the fed state on signalling molecule phosphorylation and protein synthesis in human muscle. J Physiol 586, 3701–3717. 10.1113/jphysiol.2008.153916. [PubMed: 18556367]

82. Kraemer WJ, and Ratamess NA (2005). Hormonal responses and adaptations to resistance exercise and training. Sports Med 35, 339–361. 10.2165/00007256-200535040-00004. [PubMed: 15831061]
83. Robbins JM, Peterson B, Schranner D, Tahir UA, Rienmüller T, Deng S, Keyes MJ, Katz DH, Beltran PMJ, Barber JL, et al. (2021). Human plasma proteomic profiles indicative of cardiorespiratory fitness. Nat Metab 3, 786–797. 10.1038/s42255-021-00400-z. [PubMed: 34045743]
84. Sanford JA, Nogiec CD, Lindholm ME, Adkins JN, Amar D, Dasari S, Drugan JK, Fernández FM, Radom-Aizik S, Schenk S, et al. (2020). Molecular Transducers of Physical Activity Consortium (MoTrPAC): Mapping the Dynamic Responses to Exercise. Cell 181, 1464–1474. 10.1016/j.cell.2020.06.004. [PubMed: 32589957]
85. Moller LLV, Raun SH, Fritzen AM, and Sylow L (2022). Measurement of skeletal muscle glucose uptake in mice in response to acute treadmill running. J Biol Methods 9, e162. 10.14440/jbm.2022.385. [PubMed: 36404875]
86. Perez-Riverol Y, Bai J, Bandla C, García-Seisdedos D, Hewapathirana S, Kamatchinathan S, Kundu DJ, Prakash A, Frericks-Zipper A, Eisenacher M, et al. (2022). The PRIDE database resources in 2022: a hub for mass spectrometry-based proteomics evidences. Nucleic Acids Res 50, D543–D552. 10.1093/nar/gkab1038. [PubMed: 34723319]
87. Gombash Lampe SE, Kaspar BK, and Foust KD (2014). Intravenous injections in neonatal mice. J Vis Exp, e52037. 10.3791/52037. [PubMed: 25407048]
88. Amodei D, Egertson J, MacLean BX, Johnson R, Merrihew GE, Keller A, Marsh D, Vitek O, Mallick P, and MacCoss MJ (2019). Improving Precursor Selectivity in Data-Independent Acquisition Using Overlapping Windows. J Am Soc Mass Spectrom 30, 669–684. 10.1007/s13361-018-2122-8. [PubMed: 30671891]
89. Adusumilli R, and Mallick P (2017). Data Conversion with ProteoWizard msConvert. Methods Mol Biol 1550, 339–368. 10.1007/978-1-4939-6747-6_23. [PubMed: 28188540]
90. Ting YS, Egertson JD, Bollinger JG, Searle BC, Payne SH, Noble WS, and MacCoss MJ (2017). PECAN: library-free peptide detection for data-independent acquisition tandem mass spectrometry data. Nat Methods 14, 903–908. 10.1038/nmeth.4390. [PubMed: 28783153]
91. Consortium U (2021). UniProt: the universal protein knowledgebase in 2021. Nucleic Acids Res 49, D480–D489. 10.1093/nar/gkaa1100. [PubMed: 33237286]
92. Mellacheruvu D, Wright Z, Couzens AL, Lambert JP, St-Denis NA, Li T, Miteva YV, Hauri S, Sardiu ME, Low TY, et al. (2013). The CRAPome: a contaminant repository for affinity purification-mass spectrometry data. Nat Methods 10, 730–736. 10.1038/nmeth.2557. [PubMed: 23921808]
93. Bourgon R, Gentleman R, and Huber W (2010). Independent filtering increases detection power for high-throughput experiments. Proc Natl Acad Sci U S A 107, 9546–9551. 10.1073/pnas.0914005107. [PubMed: 20460310]
94. Ashburner M, Ball CA, Blake JA, Botstein D, Butler H, Cherry JM, Davis AP, Dolinski K, Dwight SS, Eppig JT, et al. (2000). Gene ontology: tool for the unification of biology. The Gene Ontology Consortium. Nat Genet 25, 25–29. 10.1038/75556. [PubMed: 10802651]
95. Jiang Z, Zhao M, Voilquin L, Jung Y, Aikio MA, Sahai T, Dou FY, Roche AM, Carcamo-Orive I, Knowles JW, et al. (2021). Isthmin-1 is an adipokine that promotes glucose uptake and improves glucose tolerance and hepatic steatosis. Cell Metab 33, 1836–1852.e1811. 10.1016/j.cmet.2021.07.010. [PubMed: 34348115]
96. Li VL, He Y, Contrepois K, Liu H, Kim JT, Wiggenhorn AL, Tanzo JT, Tung AS, Lyu X, Zushin PH, et al. (2022). An exercise-inducible metabolite that suppresses feeding and obesity. Nature 606, 785–790. 10.1038/s41586-022-04828-5. [PubMed: 35705806]
97. Smith CA, Want EJ, O'Maille G, Abagyan R, and Siuzdak G (2006). XCMS: processing mass spectrometry data for metabolite profiling using nonlinear peak alignment, matching, and identification. Anal Chem 78, 779–787. 10.1021/ac051437y. [PubMed: 16448051]
98. Ross MK, and Borazjani A (2007). Enzymatic activity of human carboxylesterases. Curr Protoc Toxicol Chapter 4, Unit 4.24. 10.1002/0471140856.tx0424s33.

99. Alvarez-Castelao B, Schanzenbächer CT, Hanus C, Glock C, Tom Dieck S, Dörrbaum AR, Bartnik I, Nassim-Assir B, Ciirdaeva E, Mueller A, et al. (2017). Cell-type-specific metabolic labeling of nascent proteomes in vivo. Nat Biotechnol 35, 1196–1201. 10.1038/nbt.4016. [PubMed: 29106408]

100. Ritchie ME, Phipson B, Wu D, Hu Y, Law CW, Shi W, and Smyth GK (2015). limma powers differential expression analyses for RNA-sequencing and microarray studies. Nucleic Acids Res 43, e47. 10.1093/nar/gkv007. [PubMed: 25605792]

101. Law CW, Alhamdoosh M, Su S, Dong X, Tian L, Smyth GK, and Ritchie ME (2016). RNA-seq analysis is easy as 1–2-3 with limma, Glimma and edgeR. F1000Res 5. 10.12688/f1000research.9005.3.

102. Smyth GK (2004). Linear models and empirical bayes methods for assessing differential expression in microarray experiments. Stat Appl Genet Mol Biol 3, Article3. 10.2202/1544-6115.1027.

Highlights:

- An organism-wide cell type-specific secretome atlas after exercise training in mice
- Exercise training induces cell type-specific and bidirectional secretome changes
- *Pdgfra*+ cells are highly responsive to exercise training
- Secreted CES2 proteins improve metabolic health and enhance running endurance

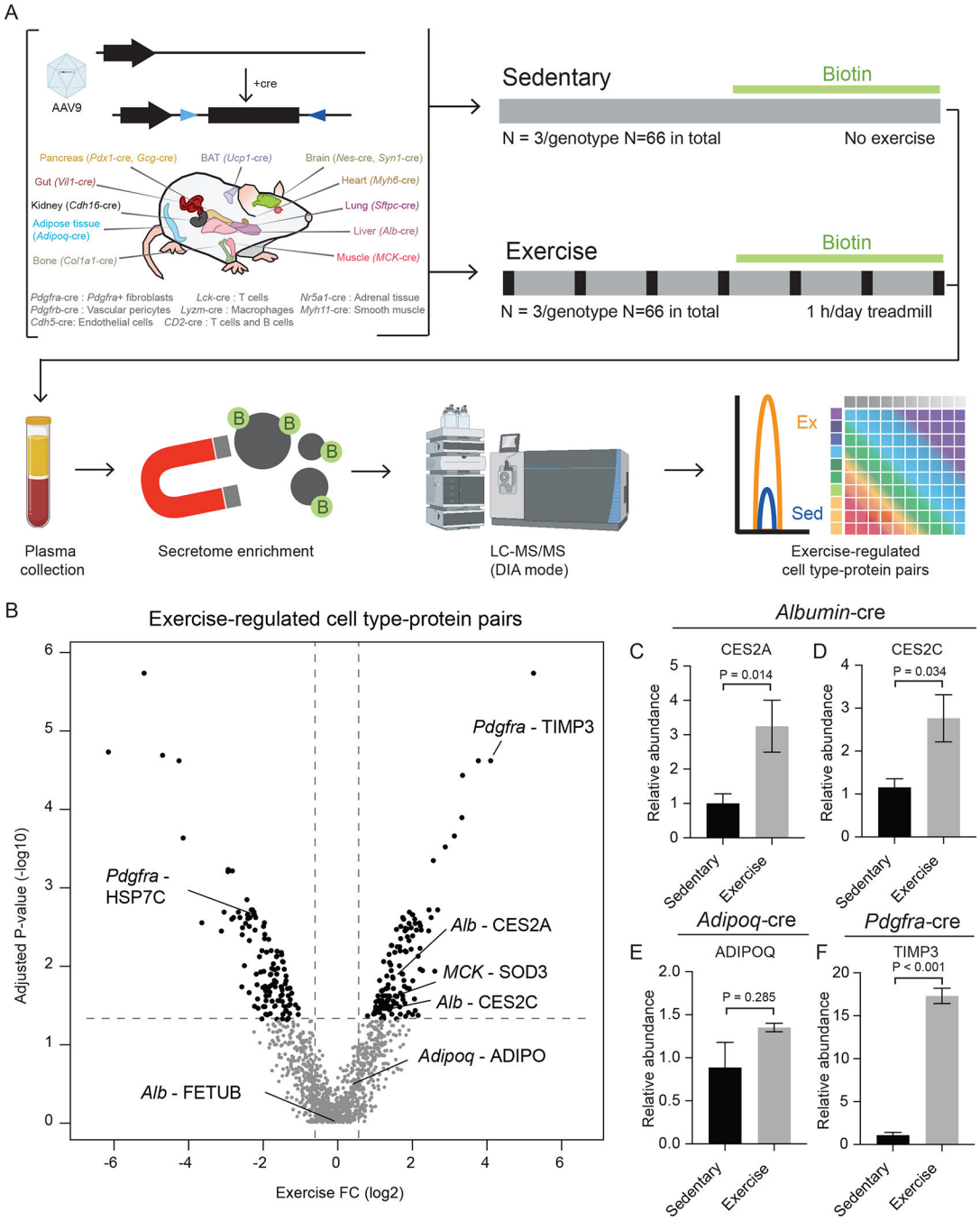

Fig 1. Study design and overview of exercise training secretomes across 21 cell types in mice.

(A) Overview of the study design including viral transduction (AAV9-FLEx-ER-TurboID, 3*10e11 GC/mouse, intravenously) of 21 cre driver lines (male, N = 3/condition/genotype, see Methods) and wildtype C57BL/6 mice (male, N = 3/condition), 1-week treadmill running (20 m/min for 60min per day), secretome labeling (biotin delivered via biotin water (0.5 mg/ml) and via injection (24 mg biotin/ml, intraperitoneally, in a solution of 18:1:1 saline:Kolliphor EL:DMSO, final volume of 200 µl per mouse per day) in the last three

days of running), enrichment of biotinylated plasma proteins using streptavidin beads and proteomic analysis. BAT: brown adipose tissue.

(B) Volcano plot of adjusted P-values (−log10) and exercise fold change (log2) of total 1272 cell type-protein pairs. Adjusted P-values were calculated from moderated t-statistics (see **Methods**). Black dots indicate exercise-regulated cell type-protein pairs (adjusted P-values < 0.05 and exercise fold change > 1.5) and gray dots indicate unchanged cell type-protein pairs (adjusted P-values > 0.05 or exercise fold change < 1.5).

(C-F) Relative abundance of exercise training -regulated (C, D and F) and exercise training-unregulated (E) cell type-protein pairs from exercise and sedentary mice. N = 3/genotype/condition, mean ± SEM. In (C-F), P-values were calculated from two-tailed unpaired t-tests.

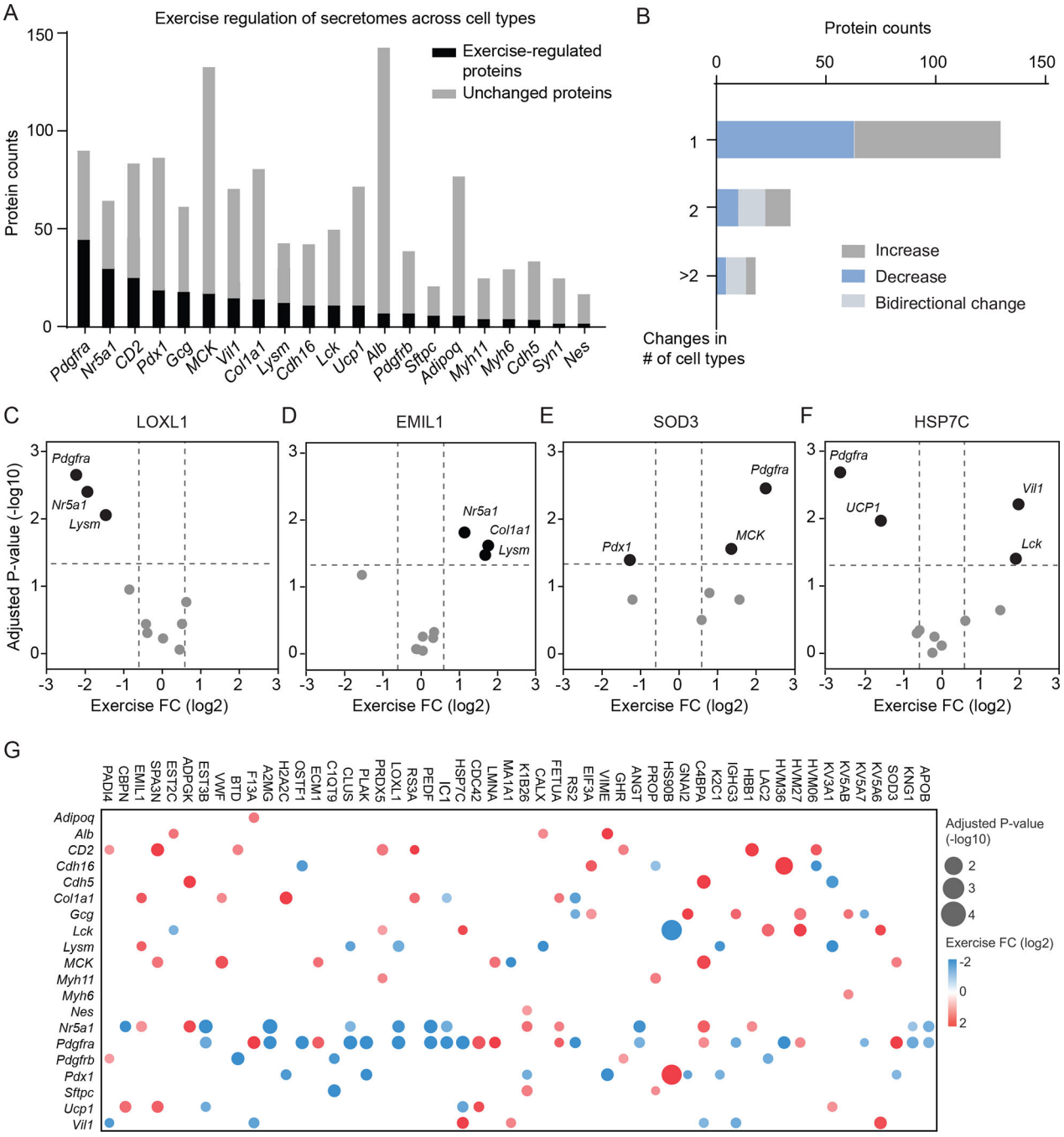

Fig 2. Systematic analysis of exercise training-regulated cell type-protein pairs.

(A) Bar graph of exercise training-regulated proteins (black) and unchanged proteins (gray) across 21 cell types.

(B) Histogram of increased (gray), decreased (blue) and bidirectionally changed (light gray) secreted proteins after exercise training across 21 cell types.

(C-F) Volcano plot of adjusted P-values (−log10) and exercise fold change (log2) of indicated example proteins. Black dots indicate exercise training-regulated cell type-protein

pairs (adjusted P-values < 0.05 and exercise fold change > 1.5) and gray dots indicate unchanged cell type-protein pairs (adjusted P-values > 0.05 or exercise fold change < 1.5). (G) Bubble plot of adjusted P-values (−log10) and exercise fold change (log2) of proteins changed in more than 1 cell type after exercise training. Red dots indicate increased proteins after exercise training and blue dots indicated decreased proteins.

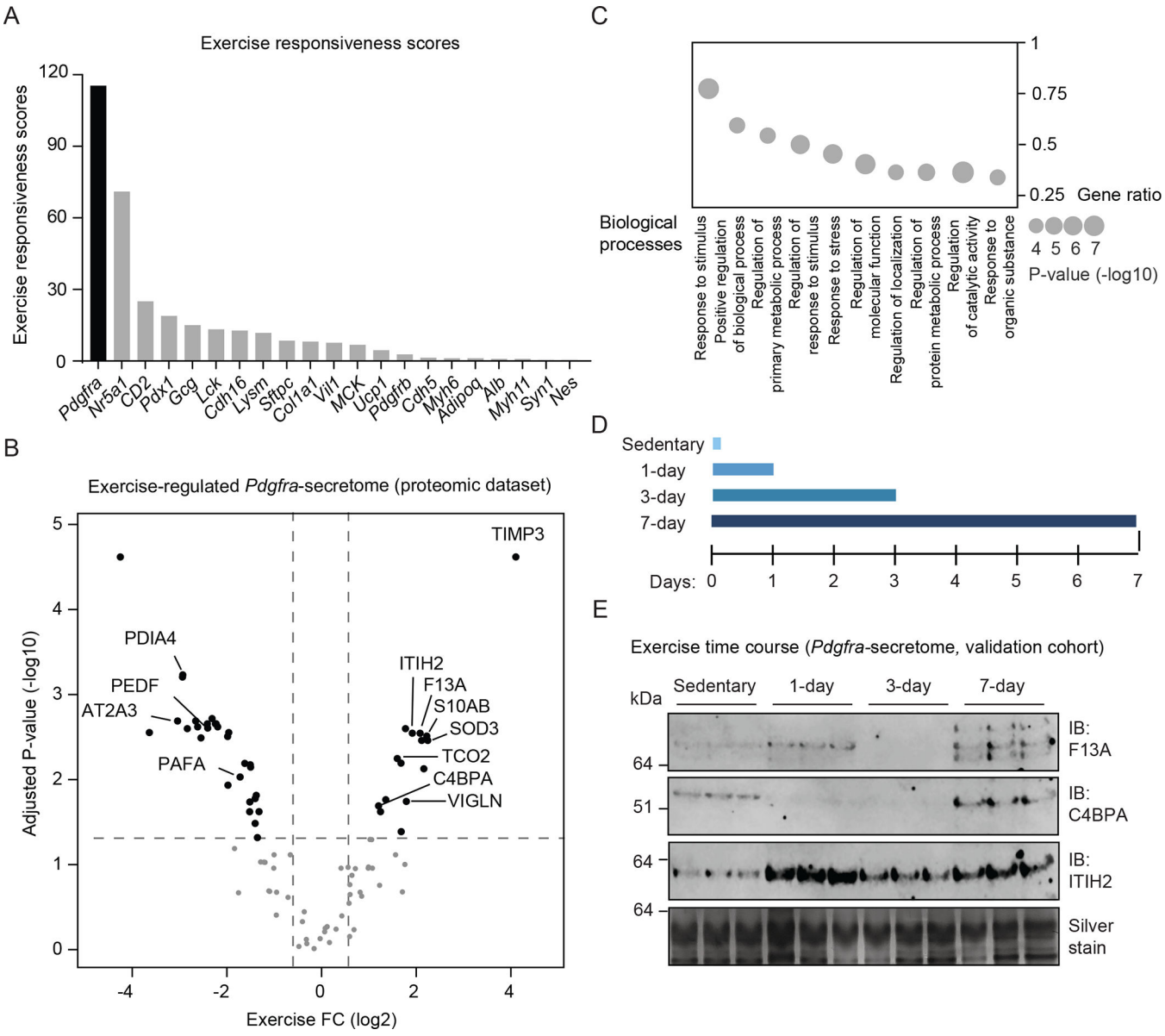

Fig 3. Characterizations of exercise training secretomes from *Pdgfra*-cre labeled cells.

(A) Bar graph of exercise responsiveness scores across cell types. Exercise responsiveness scores of a given cell type were calculated by summarization of the score of individual exercise regulated protein (adjusted P-values < 0.05 and exercise fold change > 1.5) of that cell type with the following equation: sum(absolute exercise fold change (log2) × confidence of the change (−log10(adjusted P-values))) × percent of secretome change (number of exercise training regulated proteins (adjusted P-values < 0.05 and exercise fold change > 1.5) / total number of secreted proteins of that cell type). See **Methods**.

(B) Volcano plot of adjusted P-values (−log10) and exercise fold change (log2) of *Pdgfra* secretomes. Black dots indicate exercise training -regulated cell type-protein pairs (adjusted P-values < 0.05 and exercise fold change > 1.5) and gray dots indicate unchanged cell type-protein pairs (adjusted P-values > 0.05 or exercise fold change < 1.5).

(C) Gene ontology analysis of exercise training regulated proteins (adjusted P-values < 0.05 and exercise fold change > 1.5) from *Pdgfra* secretomes. Size of bubbles represents P-values (−log10) of biological processes enrichment and y axis represents gene ratio.
(D) Study design of secretome analysis of heterozygous *Pdgfra*-cre mice (12-week-old male, N = 3/condition) injected with 3*10e11 GC/mouse AAV9-FLEx-ER-TurboID and tamoxifen. Three weeks after tamoxifen delivery, these mice were subjected to acute running (single bout, 20 m/min for 60 min), 3-day or 7-day treadmill running (daily, 20 m/min for 60 min) or being sedentary. Secretome labeling was initiated via injection (24 mg biotin/ml, intraperitoneally, in a solution of 18:1:1 saline:Kolliphor EL:DMSO, final volume of 400 μl per mouse per day) in the last bout of running and biotinylated plasma proteins were enriched using streptavidin beads and analyzed by western blotting (see **Methods**).
(E) Anti-F13A (top), anti-C4BPA (second row), anti-ITIH2 (third row) of eluted biotinylated plasma proteins from streptavidin beads after immune purification. Silver stain of total eluted biotinylated plasma proteins was used as loading control and for quantifications (bottom row). Samples (N = 3/condition) were from the experiment described in the legend of Fig. 3D.

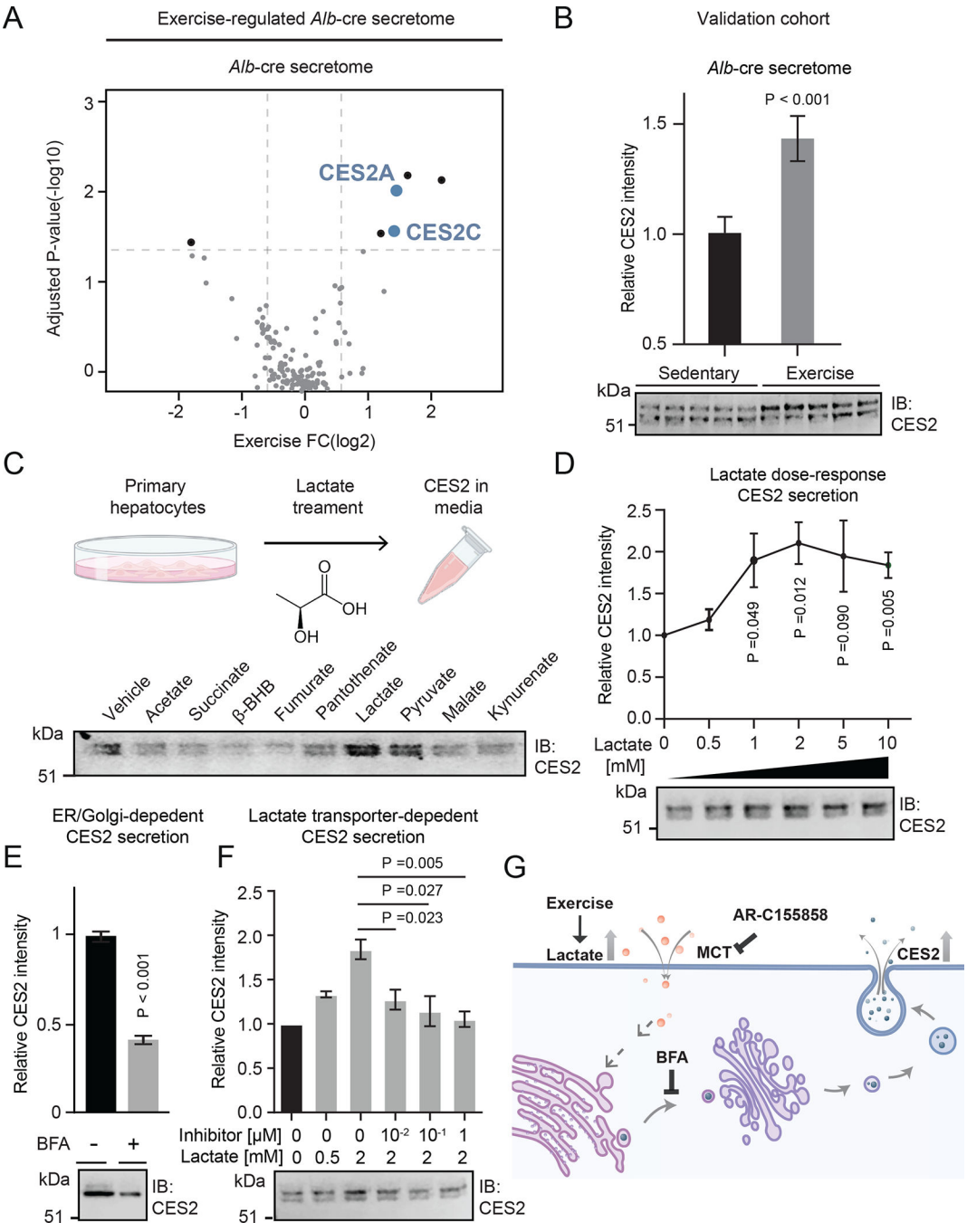

Fig 4. Lactate-induced CES2 secretion in mouse primary hepatocytes.

(A) Volcano plot of adjusted P-values (−log10) and exercise fold change (log2) of Albumin secretomes. Black dots indicate exercise training-regulated cell type-protein pairs (adjusted P-values < 0.05 and exercise fold change > 1.5) and gray dots indicate unchanged cell type-protein pairs (adjusted P-values > 0.05 or exercise fold change < 1.5).

(B) Anti-CES2 (bottom) blotting and quantifications of band intensity (top) of immune purified biotinylated plasma proteins from 10-week-old *Albumin*-cre male mice transduced

with 3*10e11 vg AAV9-FLEx-ER-TurboID virus and exercised on a treadmill for 1-week. N = 5/group, mean ± SEM.

(C-F) Anti-CES2 blotting (bottom) and quantifications of band intensity (D-F) of conditioned medium of primary hepatocytes isolated from 8 to 12-week-old male C57BL/6J mice. Cells were treated with 2 mM indicated organic compounds (C), indicated concentrations of sodium lactate (D), sodium lactate (2 mM) and BFA (5 μg/ml) (E), indicated concentrations of sodium lactate and AR-C155858 (F) for 4 h before analysis. CES2 band intensity was normalized to albumin signal for quantifications. Experiments in each panel contains three biological replicates, mean ± SEM.

(G) Model of CES2 secretion from cells. Exercise training-inducible rise of extracellular lactate induces release of ER-lumen-resident CES2 from hepatocytes. Functional lactate transporters and ER-Golgi vesicle transport are required for CES2 secretion.

P-values for quantifications in this figure were calculated from two-tailed unpaired t-tests.

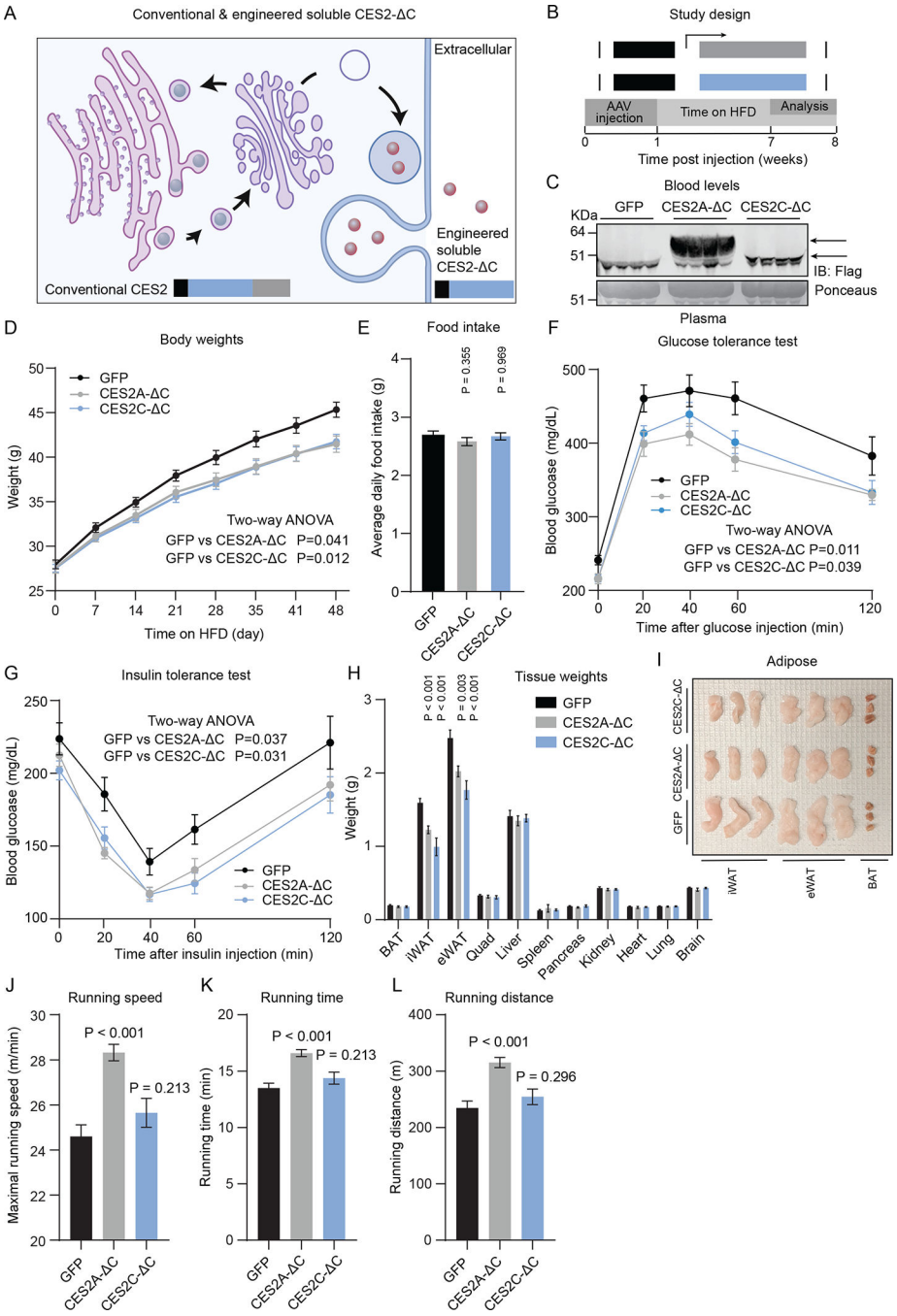

Fig 5. Secreted CES2 proteins exhibit anti-obesity, and anti-diabetic, and endurance-enhancing effects in mice.

(A) Cartoon schematic of conventional ER lumen localized CES2A/C (left) and engineered CES2A/C-ΔC (right). The C-terminal HXEL sequence was removed from conventional CES2A/C to generate engineered soluble CES2A/C-ΔC.

(B) Cartoon schematic of the AAV constructs driven by the hepatocyte-specific *Tbg* promoter and study design of HFD feeding experiment. 8 to 10-week-old male C57BL/6 mice were transduced with AAV-*Tbg*-CES2A-ΔC or AAV-*Tbg*-CES2C-ΔC or AAV-*Tbg*-GFP (N = 10/group, 10e11 GC/mouse, intravenously). 1-week later, mice were placed with

HFD feeding for 7 weeks. In the last week, glucose tolerance test and insulin tolerance test were conducted. At the end of this experiment, tissues and blood were harvested and analyzed.

(C) Anti-Flag blotting (top) or loading control (bottom) of blood plasma from 16 to 18-week-old male C57BL/6 mice injected with indicated viruses. N = 4/condition.

(D-I) Body weights over the first 7-week of HFD feeding (D) and food intake (measured weekly) (E), glucose tolerance test (F), insulin tolerance test (G), tissue weights (H) and inguinal white adipose tissue (iWAT), epididymal adipose tissue (eWAT) and brown adipose tissue (BAT) after 48 h of 4% PFA fixation (I) from 16 to 18-week-old male C57BL/6 mice injected with indicated viruses for 8 weeks. N = 10/condition, mean ± SEM. Samples from (I) were from randomly chosen from mice of each treatment group.

(J-L) Maximal running speed (J), total running time (K) and total running distance (L) of 16 to 18-week-old male C57BL/6 mice 8 weeks after being injected with AAV-*Tbg*-CES2A-ΔC, AAV-*Tbg*-CES2C-ΔC or AAV-*Tbg*-GFP (N = 8–10/group, 10e11 GC/mouse, intravenously). Mice were acclimated to the treadmill two days prior to the maximal running tests (10 min at 10 m/min). The maximal running test was performed as previously described[70,85] (see **Methods**). Mean ± SEM.

P-values for (E), (H) and (J-L) were calculated from two-tailed unpaired t-tests. P-values from (D), (F) and (G) were calculated from two-way ANOVA with post hoc Sidak's multiple comparisons test.

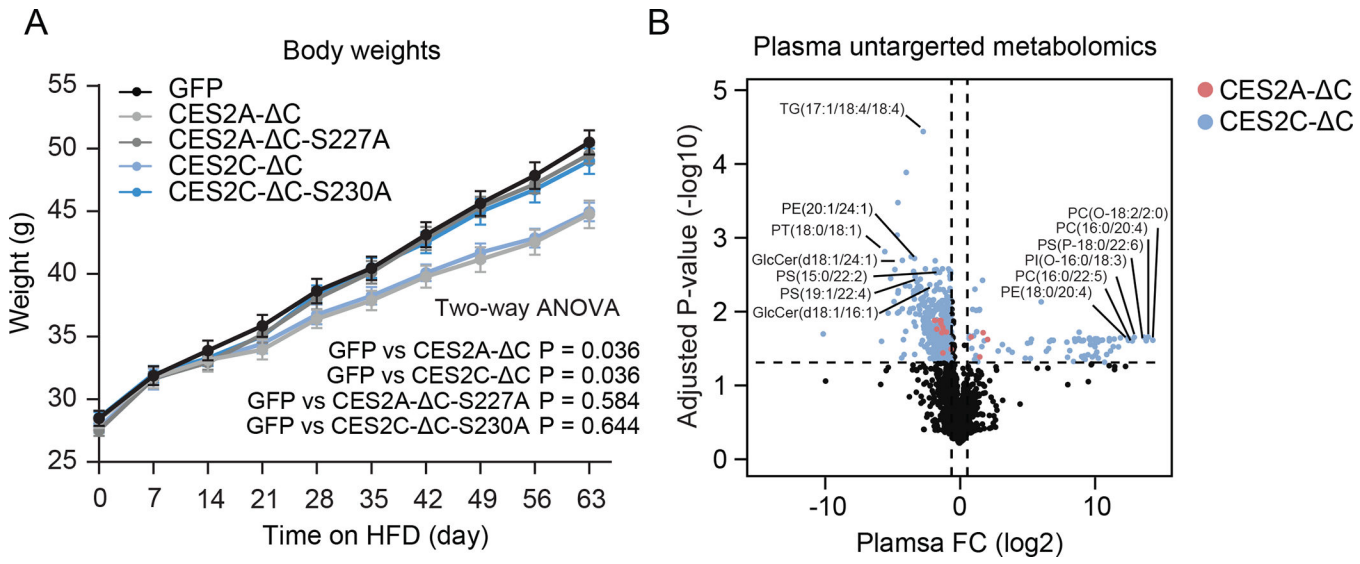

Fig 6. The anti-obesity effects of soluble CES2 proteins require enzyme activity.

(A) Body weights over the first 9-week of HFD feeding of 18 to 20-week-old male C57BL/6 mice injected with indicated viruses (N = 10/group, 10e11 GC/mouse, intravenously). Mice were fed with HFD 1-week after viral transduction. Mean ± SEM.

(B) Untargeted metabolomic measurements of significantly changed features (adjusted P-values < 0.05 and fold change > 1.5) in blood plasma of 16 to 18-week-old male C57BL/6 mice being transduced with 10e11 AAV-*Tbg*-CES2A-ΔC, AAV-*Tbg*-CES2C-ΔC or AAV-*Tbg*-GFP (N = 5/group). Mice were placed with HFD feeding for 7 weeks before LC-MS analysis (see **Methods**).

P-values for (A) were calculated from two-way ANOVA with post hoc Sidak's multiple comparisons test.

Key resources table

REAGENT or RESOURCE	SOURCE	IDENTIFIER
Antibodies		
Anti-V5 antibody (1:1000 dilution)	Invitrogen	R960-25
Anti-Flag antibody (1:1000 dilution)	Sigma	F1804
Anti- β Tubulin (1:5000 dilution)	Abcam	ab6046
Anti-CES2 (1:1000 dilution)	Novus Biologicals	NBP1-91620
Anti-TIMP3 (1:500 dilution)	Thermo Fisher	710404
Anti-F13A (1:500 dilution)	MyBioSource	MBS2026456
Anti-ITIH2 (1:500 dilution)	MyBioSource	MyBioSource
Anti-C4BPA (1:500 dilution)	Abnova	H00000722-D01P
Anti-mouse IgG IRDye 680RD (1:10000 dilution)	LI-COR	925-68070
Anti-rabbit IgG IRDye 800RD (1:10000 dilution)	LI-COR	926-32211
Anti-biotin Streptavidin AlexaFluor680 (1:1000 dilution)	ThermoFisher	S32358
FITC anti-Mouse TCRβ	BioLegend	109206
PerCP/Cy5.5 anti-Mouse CD19 antibody	BioLegend	152406
Anti-mouse albumin (1:5000 dilution)	Novus Biologicals	NB600-41532
Anti-BHMT (1:1000 dilution)	Abcam	ab96415
Anti-goat IgG IRDye 800CW (1:10000 dilution)	LI-COR	925-32214
Recombinant DNA		
pAAV-FLEx-ER-TurboID plasmid	Addgene	160857
pAAV-*Tbg*-ER-TurboID plasmid	Addgene	149415
pDEST40-CES2A-ΔC expression plasmid	This paper	N/A
pDEST40-CES2C-ΔC expression plasmid	This paper	N/A
pDEST40-CES2A-ΔC-S227A expression plasmid	This paper	N/A
pDEST40-CES2C-ΔC-S230A expression plasmid	This paper	N/A
pAAV-*Tbg*-CES2A-ΔC plasmid	This paper	N/A
pAAV-*Tbg*-CES2C-ΔC plasmid	This paper	N/A
pAAV-*Tbg*-CES2A-ΔC-S227A plasmid	This paper	N/A
pAAV-*Tbg*-CES2C-ΔC-S230A plasmid	This paper	N/A
Chemicals, Peptides, and Recombinant Proteins		
Biotin	Sigma	B4501-1G
DTT	Sigma	D0632-1G
4-nitrophenyl acetate	Sigma	N8130-5G
D-(+)-Glucose	Sigma	50-99-7
DPBS	Thermo Fisher	14190144
Human recombinant insulin	Sigma	91077C
Dexamethasone	Sigma	D4902-100MG
Rosiglitazone	Cayman	71740
IBMX	Sigma	I-5879

REAGENT or RESOURCE	SOURCE	IDENTIFIER
BSA	Sigma	A7906-500G
Sodium azide	Sigma	S2002-25G
Sodium chloride	Sigma	S9888-500G
Sodium deoxycholate	Sigma	D6750-100G
Sodium dodecyl sulfate	Thermo Fisher	BP166-500
Sodium carbonate	Thermo Fisher	S263-500
Sodium bicarbonate	Thermo Fisher	187508
Sodium ascorbate	Thermo Fisher	A0539500G
Sodium L-lactate	Sigma	L7022-5G
Sodium fumarate dibasic	Sigma	F1506-25G
Sodium succinate dibasic hexahydrate	Sigma	S2378-100G
Sodium (R)-3-hydroxybutyrate	Sigma	298360-1G
Kynurenic acid	Sigma	K3375-250MG
D-Pantothenic acid hemicalcium salt	Sigma	21210-5G-F
Sodium pyruvate	Sigma	P2256-25G
L-(−)-Malic acid	Sigma	02288-10G
Dimethyl sulfoxide	Sigma	D8418-100ML
Potassium chloride	Sigma	P3911-500G
EDTA	Sigma	E9884-100G
EDTA, 0.5 M, pH 8.0	EMD Millipore	324506
Tris-HCl	Sigma	1185-53-1
Acetonitrile	Thermo Fisher	A998-4
Alcohol ethyl ethanol 200 proof	Gold Shield Distributors	0412804-PINT
HALT protease inhibitor	Thermo Fisher	78429
NP-40 alternative	MIllipore	492016-100ML
Chloroform	Thermo Fisher	C607-4
Ponceau S solution	Sigma	P7170-1L
NuPAGE MOPS SDS Running Buffer (20X)	Invitrogen	NP0001-02
NuPAGE 4-12% Bis-Tris Protein Gels, 1.0 mm, 15-well	Thermo Fisher	NP0323BOX
Odyssey blocking buffer	LI-COR	927-50000
Seeblue plus 2 protein ladder	Thermo Fisher	LC5925
NuPAGE™ LDS Sample Buffer (4X)	Thermo Fisher	NP0008
Urea	Sigma	31K0038
Acetone	Thermo Fisher	A184
Formic acid	Thermo Fisher	A117-50
Phosphoric acid	Sigma	345245-100ML
Trolox	Sigma	648471-500MG
0.9% saline solution	Teknova	S5825
TEAB solution (1M)	Sigma	T7408-100ML

REAGENT or RESOURCE	SOURCE	IDENTIFIER
Kolliphor EL	Sigma	C5135-500G
Pierce™ 16% Formaldehyde (w/v), Methanol-free	Thermo Fisher	28908
Trypsin	Promega	V5113
Iodoacetamide	Sigma	A3221
Brefeldin A0	Sigma	B6542-5MG
AR-C155858	Tocris	4960
Critical Commercial Assays		
SilverQuest™ Silver Staining Kit	Thermo Fisher	LC6070
Trans-blot turbo RTA transfer kit, nitrocellulose	Biorad	1704271
LIVE/DEAD™ Fixable Aqua Dead Cell Stain Kit	Invitrogen	L34957
RNeasy Mini Kit	Qiagen	74106
Q5® Site-Directed Mutagenesis Kit	NEB Biolabs	E0554S
High-Capacity cDNA Reverse Transcription Kit	Thermo Fisher	4368813
Experimental Models: Organisms/Strains		
C57BL/6J (M. musculus)	Jackson Laboratory	000664
Alb-cre mice	Jackson Laboratory	003574
Cdh16-cre mice	Jackson Laboratory	012237
Gcg-icre mice	Jackson Laboratory	030663
Pdx1-cre mice	Jackson Laboratory	014647
Myh6-creER mice	Jackson Laboratory	005657
MCK-cre mice	Jackson Laboratory	006475
Myh11-icreER mice	Jackson Laboratory	019079
Cdh5-cre mice	Jackson Laboratory	006137
Pdgfra-creER mice	Jackson Laboratory	032770
Pdgfrb-creER mice	Jackson Laboratory	030201
Vil1-cre mice	Jackson Laboratory	021504
Sftpc-creER mice	Jackson Laboratory	028054
Col1a1-creER mice	Jackson Laboratory	016241
CD2-icre mice	Jackson Laboratory	008520
Lck-cre mice	Jackson Laboratory	003802
Nr5a1-cre mice	Jackson Laboratory	033687
Nes-creER mice	Jackson Laboratory	016261
Syn1-cre mice	Jackson Laboratory	003966
Adipoq-cre mice	Jackson Laboratory	028020
Ucp1-cre mice	Jackson Laboratory	024670
LysM-creER mice	Jackson Laboratory	032291
Experimental Models: Cell Lines		
HEK293T cells	ATCC	CRL-3216
Primary mouse hepatocytes	This paper	N/A

REAGENT or RESOURCE	SOURCE	IDENTIFIER
Bacterial and Virus Strains		
One Shot™ TOP10 Chemically Competent E. coli	Invitrogen	C404010
AAV9-FLEx-ER-TurboID	UPenn Vector Core	60221S
AAV8-*Tbg*-GFP	Addgene	105535-AAV8
AAV8-*Tbg*-CES2A-ΔC	UPenn Vector Core	63849S
AAV8-*Tbg*-CES2C-ΔC	UPenn Vector Core	63850S
AAV8-*Tbg*-CES2A-ΔC-S227A	UPenn Vector Core	V7929S
AAV8-*Tbg*-CES2C-ΔC-S230A	UPenn Vector Core	V7928S
Oligonucleotides		
See Table S7		
Deposited Data		
Proteomic data	This study	ProteomeXchange: PXD021602
Processed proteomic datasets	Wei, Riley et al. (2021)	N/A
Other		
3 kDa Molecular Weight Cutoff Filter	Amicon	UFC9003
pENTR/D-TOPO Cloning Kit	Invitrogen	K240020
Gateway LR Clonase Enzyme mix	Invitrogen	11791019
Gibson Assembly Master Mix	NEB Biolabs	E2611L
Phusion High-Fidelity PCR Master Mix with HF Buffer	NEB Biolabs	M0531L
ExpiFectamine 293 Transfection Kit	Thermo Fisher	A14524
His GraviTrap TALON	Cytiva	29-0005-94
QIAquick gel extraction kit	Qiagen	28704
EndoFree Plasmid Maxi Kit	Qiagen	12362
NotI	NEB Biolabs	R3189S
HindIII	NEB Biolabs	R3104S
EcoRV	NEB Biolabs	R3195S
XhoI	NEB Biolabs	R0146S
HFD with 60 kcal% fat	ResearchDiets	D12492
Thioglycollate Medium Brewer Modified	Thermo Fisher	B11716
Collagen I, Rat	Corning	CB-40236
Dispase II	Roche	04942078001
Collagenase D	Roche	11088882001
Collagenase IV	Sigma	C5138-1G
Percoll	Sigma	P4937-500ML
10x PBS	Gibco	70011044
HBSS buffer	Gibco	14175-095
Williams E media	Quality Biological	10128-636
Corning Regular Fetal Bovine Serum	Corning	35-010-CV
DMEM	Corning	10-017-CV

REAGENT or RESOURCE	SOURCE	IDENTIFIER
DMEM/F12 (1:1)	Gibco	11320082
DMEM/F-12, GlutaMAX™ supplement	Gibco	10565042
Expi293 Expression medium	Thermo Fisher	A1435101
100um cell strainer	Falcon	352360
70um cell strainer	Falcon	352350
S-Trap™ micro columns	Protifi	C02-micro-80
lithium heparin tube	BD	365985
PrecisionGlide Needle 21G	BD	305129
Exel International Insulin Syringes 29G	Exel International	14-841-32
Ultrafine Insulin Syringes 31G	BD	328290
Trypan blue solution 0.4%	Invitrogen	15250061
Ultra Sensitive Mouse Insulin ELISA Kit	Crystal Chem	90080
Triglyceride colorimetric assay kit	Cayman	10010303
Pierce BCA Protein Assay Kit	Thermo Fisher	23225
Tailveiner Restrainer for Mice	Braintree	TV-150 STD
Streptavidin magnetic beads	Thermo Fisher	65601
Blood Glucose meter	OneTouch UltraMini meter	N/A
Blood Glucose Strips	GenUltimate	100-50
96-Well Microplate Fisherbrand	Fisher Scientific	12565501
TRIzol Reagent	Invitrogen	15596026
Ssoadvance Universal SYBR Green mix	Biorad	1725272
Bulk tubes	Thermo Fisher	15340162
Metal Bulk Beads	Thermo Fisher	15340158
Benchmark BeadBlaster Homogenizer	Thermo Fisher	15-340-163
Orbitrap Fusion Tribrid Mass Spectrometer	Thermo Fisher	N/A
Agilent 6470 triple quadrupole LC-MS instrument	Agilent	N/A
NH2 100 Å LC column	Phenomenex	00B-4378-E0